THE PRESSURE LOSSES IN 90° BENDS

THE PRESSURE LOSSES IN 90° BENDS

OF

RECTANGULAR CROSS SECTION

by

SURESH CHANDRA KACKER, B.TECH.

A Thesis

Submitted to the Faculty of Graduate Studies

in Partial Fulfilment of the Requirements

for the Degree

Master of Engineering

McMaster University
October, 1966

MASTER OF ENGINEERING (1966)   McMASTER UNIVERSITY
(Mechanical)   Hamilton, Ontario

TITLE: The Pressure Losses in 90° Bends of Rectangular Cross-section

AUTHOR: Suresh Chandra Kacker, B.Tech. (Indian Institute of Technology,
                                          Kanpur, India)

SUPERVISOR: Dr. J. H. T. Wade

NUMBER OF PAGES: vi, 96

SCOPE & CONTENTS:

An experimental study of the turbulent flow of air around a
90° bend is reported in this thesis. Four 90° bends of aspect ratio
1, 3, 5 & 10 and radius ratio 1.0 have been tested in the Reynolds
number range from 1×10^5 to 5×10^5. The loss in total pressure
across the bend (or elbow) is reported for two discharge conditions
(1) the elbow discharging to a plenum chamber through a constant area
duct of a length equal to 4 hydraulic diameters; (2) the elbow dis-
charging to the plenum chamber directly. A comparison of the experi-
mental results is made with the curves given in NACA report L4F26 which
have been reproduced in the recently published SAE Aero-Space Manual.

Various other flow parameters, such as velocity profiles, tur-
bulence levels and pressure distributions are also given in this thesis.

ii

ACKNOWLEDGMENTS

TABLE OF CONTENTS

LIST OF FIGURES

List of Figures (continued)

TEXT

CHAPTER I

INTRODUCTION

At the present time data concerning the loss coefficient across elbows is available from a number of publications probably the most recent of which is the SAE Aero-Space Manual which supersedes an earlier SAE report No. 23. Both the above mentioned references give the curves for the ratio of loss in total pressure to the duct dynamic pressure as a function of aspect ratio, radius ratio and Reynolds number. These curves have been taken from an early NACA report L4F26 written by J. R. Henry in 1944. Henry in his report mentions that the curves are based upon the work of five different workers in this field. A survey of the literature reveals that the curves are not totally experimental and because of the large number of parameters involved interpolation and extrapolation was necessary of the experimental results to provide the families of curves given in these reports. On further examination of the experimental points, it was felt that the family of the curves may be only approximately correct since it was obvious that curves of other shapes could be drawn through the experimental points. With this in mind, it was proposed to start a research program to more clearly define the shape of the pressure loss curves as a function of Reynolds number, radius ratio and aspect ratio.

The present work deals with the determination of the total pressure loss coefficient obtained by testing four 90° elbows of 24" x 24", 24" x 8", 24" x 4.8" and 24" x 2.4" cross section and radius

ratio of 1.0, over a range of Reynolds number from 1×10^5 to 5×10^5.
It has been observed by previous workers that both the inlet and exit
condition affect the performance of the flow in the elbow. It was
therefore felt necessary to test the bend under at least two exit con-
ditions. In the first configuration the elbow discharged to a plenum
chamber through a straight duct of constant cross section having a
length equal to 4 hydraulic diameters. The second configuration tested
was that of the 90° bend exhausting directly to a plenum chamber. The
present tests define the inlet conditions to the bend and includes
measurements of the pressure distributions along the walls, the velocity
profile entering the bend and the turbulence level of the free stream.

CHAPTER II

LITERATURE SURVEY

The information available to the researcher in the area is comprehensive. A National Research Council sub-committee has recently undertaken a literature survey in the field of internal aero dynamics which includes bend performance and has compiled over 100 references dealing with some aspect of the flow around a bend. The survey, which has not as yet been published, shows that the workers in this field were primarily concerned with two aspects of the flow:-

1. The loss in total pressure as the flow is turned through an angle, in general 90°.

2. Theoretical and experimental investigations of the velocity field, including the secondary flow, in an elbow.

Only those reports which it is felt have a direct bearing on the present experimental work are discussed in the literature survey to follow.

1. Loss in total pressure

The experimental methods which have been used by the workers to find the loss in total pressure across the elbow are of two basic types:-

(a) Deduction method

(b) Interposition method

In the Deduction method the pressure loss was measured across

a duct system containing an elbow between two straight sections. The loss due to the elbow was then obtained by deducting the calculated friction loss over the straight lengths from the overall measured pressure loss. In the Interposition method the energy loss between two stations on a straight run of duct was obtained at a given velocity head, then an elbow was interposed in the straight run and the loss again obtained between the two stations for the same head. The difference between the two losses was considered to be the loss due to the elbow. It can be seen that the two methods only differ in the way in which the straight lengths of pipe are taken into account. The Interposition method is probably more accurate especially where the interior surface of the sections cannot be properly defined.

One of the earliest works reported in the field was done by F. L. Busey (1)[*] in 1913. He tested round elbows 12 inches in diameter and square elbows of 12" x 12" cross section. The radius ratio varied from 0 to 3.0 (a radius ratio of 0 corresponded to a square turn elbow having inside and outside corners square, whereas a radius ratio of 0.5 to 0.75 was termed by him as a short bend having the inside corner square and the outside corner round). He essentially used the Interposition method to find the losses. The air tight box used in the experiment had a short straight outlet pipe to which an elbow was fitted having a straight exit duct with a length of 3 diameters. Losses were measured by noting the increase in the static pressure (obtained by running the fan at a higher speed) in the air box required to keep the velocity head in the discharge pipe constant when the elbow was inter-

[*]The numbers in parenthesis indicate references listed in Section 10.

posed. Results were given in the form of a curve showing the variation of velocity head lost due to elbow as a function of radius ratio. The experiment was run at a constant Reynolds number, the magnitude of which was not given.

In 1927 L. Wirt (2) extended the work of Busey in order to take into account the effect of aspect ratio. He was also able to test for different exit conditions. Here again the Interposition method was used to obtain the losses. Free stream velocities up to 1,000 ft./sec. and radius ratios of 0.5 to 2.0 were investigated. Wirt's results do not compare very favourably with Busey's results. For example, at a radius ratio of 1.0 and an aspect ratio of 1, the results quoted are 100 percent higher than Busey's results. In order to take into account the effect of aspect ratio he gave a curve showing the relation between an "aspect ratio factor" and "aspect ratio". To obtain the loss in a bend with an aspect ratio different than 1 the "aspect ratio factor" had to be multiplied to the loss at aspect ratio unity. It is to be noted that the curves were not totally experimental since some of the curves were obtained by interpolation between experimental results.

The first comprehensive work was done in 1936 by Madison and Parker (3). They pointed out the importance of taking into account the shape and size of the elbow, since the surface friction factor $\in/D$ varies with shape and size. Their apparatus and method of measuring losses were very similar to that used by Busey. The only difference being that they included a straight duct having a length equal to 20 diameters, which was required to obtain a uniform velocity before the bend. Three elbows of 9, 36 and 144 square inches cross sectional area

with radius ratios of 0.5 to 1.5 were tested. They provided a graph between velocity head loss and radius ratio with the aspect ratio taken as a third parameter (varied from 0.25 to 4.0) for a free stream velocity of 30 ft./sec. Data for low radius ratios and aspect ratios other than 1 were obtained by calculation. It was reported that the physical size had very little effect on the pressure loss coefficient. Further results were obtained at a free stream velocity of approximately 63 ft./sec. and the authors suggested on the basis of the two sets of results, that the pressure loss varied as the 1.81 power of velocity.

Unfortunately it was not possible to compare the results of the above three reports because of differences in the upstream and downstream conditions that existed for the bend. In Busey's test the elbow was only three diameters downstream from the plenum chamber and the velocity measurements were taken at a plane 2½ diameters from the chamber. Air was discharged to the atmosphere three diameters downstream from the elbow. It was entirely possible that disturbances due to the duct entry persisted to the elbow. The velocity profile entering the elbow was flat in Wirt's tests because the elbow was immediately preceded by a nozzle. In the Interposition method used by Busey[1], Parker & Madison[3] and Wirt[4] a very short duct (3 to 4 diameters length) was utilised downstream of the elbow. The possibility existed in these cases that discharging so close to the elbow might have had an appreciable effect on the measured losses.

J. R. Henry (4) published a comprehensive collection of information on pressure losses of the duct components. He gave detailed graphs for the loss of pressure in 90° bends as a function of Reynolds number, aspect ratio, and radius ratio. These graphs are for four different

types of duct cross section - square, circular, elliptical and rect-
angular and were based upon the data appearing in references 2, 6, 18,
19, 20 and 21. On the basis of the data given in reference 20 he has
quoted that the ratio of losses through two geometrically similar bends
identical except for the surface roughness, is equal to the 1.75 power
of the ratio of the friction factors. Pressure loss curves appearing
in references 22 (SAE report No. 23) and 26 (Aero-Space Manual) have
been taken from reference 4.

The first theoretical attempt to predict the losses at high
Reynolds numbers was carried out by J. R. Weske (5) in 1948. The layer
of the fluid, which is near the walls of the curved duct has been termed
by him as the "shedding layer". In this shedding layer the velocity com-
ponent in the peripheral direction is considered to be of the same order
as axial velocity component in the duct preceding the bend. In a manner
analogous to the boundary layer equations, he developed equations for
the shedding layer. He put forward a hypothesis that the net bend loss
(not including the direct friction drop) was proportional to the product
of the mass flow in the shedding layer and the dynamic head based on the
mean axial velocity. The solution of the equation of motion for the
shedding layer led to the relation for the net pressure drop in curved
ducts as a function of radius ratio and Reynolds number. The integrated
results were only of a qualitative nature. In a later paper (6) he gave
the results for the pressure losses in three elbows 5" x 5", 2" x 12"
and 9" x 3", and radius ratios 0.75, 1.5 and 4.0. A curve between
Δ P static/q (loss due to direct friction not included) and $(d/R)^2$
showed nearly a linear relation. The pressure drop Δ P static/q was

also plotted against R/ $\sqrt{a}$ for the Reynolds number range from 2×10^5 to 8×10^5.

In 1956 Higginbotham, Woods & Valentine (7) studied the effect of R/d(0.75, 1.0 and 2.5) for a 90° bend. The effect of the bend on the choking Mach number and the effect of thick and thin boundary layers at the inlet section was also reported. By the use of a relaxation method they plotted the variation of the static pressure in a 90° bend for different R/d assuming two dimensional incompressible potential flow. The experimental pressure distribution when compared with the theoretical solution showed more deviation at the inside wall of the bend than at the outside wall. They observed that the thickening of the inlet boundary layer produced somewhat less uniform distributions downstream of the elbow but did not apparently affect the pressure losses and choking Mach number.

H. Ito (8) in 1959 proposed some empirical formulae, based upon theoretical considerations for the friction factor to be used in computing the pressure losses for the turbulent flow in smooth curved pipes. His results are meant for fully developed curved flow as he used bends having nearly a 360° turning angle and radius ratios from 16.4 to 648. In 1960 he performed a set of experiments with bends of 90° and various other angles (9). The pipe diameter chosen was 3.5 cm. and the radius ratio varied from 1.25 to 14. The flow entering the bend was fully developed and the results were presented for the total bend loss coefficient in form of an empirical equation. He also introduced a group of dimensionless numbers to correlate the data.

A. J. W. Smith (10) in 1963 included Ito's work to present the

latest correlation of the data for the pressure losses in smooth pipe bends of constant cross section. He divided the bends into two groups. The first group included the bends in which a large region of fully developed curved flow was attained. All other bends having not fully developed curved flow formed the second group. The effect of Reynolds number on the pressure loss coefficient was quoted from Ito's work and is considered valid for rectangular cross sections with aspect ratios between 1 to 4. The effect of downstream discharge duct length on pressure loss coefficient has been discussed at length by the author and he has provided a graph between the pressure loss coefficient and the radius ratio with the length of the discharge duct taken as a parameter.

2. <u>Experimental & Theoretical Investigation of the Velocity Field and Secondary Flow in an Elbow</u>

Wattendorf (11) reported experimental work which he did with two channels (any rectangular duct with aspect ratio between 5 & 10 or preferably higher can be considered as a channel) of width 5 cm., height to width ratio 18:1 and r_c=20 cm. and 45 cm. The flow at the inlet of the bend was fully developed and the fluid after turning through 180° in the channel of constant curvature gave fully developed bend flow in which the high velocity region was displaced towards the inside of the bend. He did not measure the static pressure in the bend directly but derived an equation to calculate the pressure at any radius. The

equation was expressed in terms of the wall static pressure, the radius

at any point of interest and the total pressure at that point. In the

central part of the channel, the flow was nearly potential (ur=constant).

It was found that at inner wall the flow deviated much more from potential

flow than at the outer wall. He also discussed Prandtl's stability theory

regarding curved flow which stated that the flow was unstable if the pro-

duct u times r decreased with increasing r. The product u times r = con-

stant indicated neutral stability.

Wattendorf plotted the velocity profile near convex, straight and

concave channel surfaces using the Universal velocity distribution:

$$\frac{u}{v^*} = f(yv^*/\nu)$$

in which v* was calculated by a method similar to that used by Preston

(25). He also tried to establish the variation of the power law exponent

'n' with the curvature parameter $(\nu/r_c v^*)$.

J. R. Weske (12) performed quite extensive experiments on the

fluid flow in elbows of round and elliptical, as well as square and

rectangular cross section, in the range of Reynolds number from 2×10^5

to 6×10^5. One of his main areas of investigation concerned the velocity

distribution at the outlet of the elbow. His results show typical vel-

ocity distributions for a 6" diameter and 1.5 radius ratio elbow and also

for a $5\frac{5}{16}$" x $5\frac{5}{16}$" square elbow at same radius ratio and at the same Reynolds

number (5×10^5). Pitot tubes, directional pitot tubes, yaw heads and

hot wire measuring devices were used to investigate the velocity field.

He concluded that velocity distributions in curved ducts of different

cross section, shape and aspect ratio, were quite similar and that the

shape and proportions of duct section were, concerning their effect upon

the velocity pattern, a minor factor compared with the radius ratio.

Between 1954 and 1957 Eskinazi (13) and Yeh (14) reported their work on fully turbulent flow in a curved channel with special reference to their hot wire measurements. In 1954 Eskinazi performed experiments using a channel 3" wide with aspect ratio 15.5 and an inside wall radius of curvature of 30". The channel turned the flow through 300° and his results confirmed the work of Wattendorf that fully developed bend flow was obtained after a turning angle of nearly 172°. He used Wattendorf's method of calculating the static pressure at any point. He was able to calculate the stress in the flow and the null shear point with the help of $\overline{u' v'}$ turbulence measurements. The turbulence measurements showed an asymmetric turbulence profile in the fully developed curved flow with the point of the minimum turbulence shifted towards the inner surface. Later on in 1957 Yeh repeated the work with a channel in which the inside radius of curvature $(r_c) = 9"$ and the outside radius of curvature $(r_o) = 12"$ and found that the fully developed curve flow was established at 240°. He reported encountering great difficulty in maintaining a steady flow in the channel because of the method of discharge from the channel exit. He questioned his results on this very point.

The secondary flow in a curved pipe was studied by Hawthorne (15), Detra (16), Eichenberger (17) and many others. These workers were mainly concerned with the prediction of the secondary flow velocity on the basis of inviscid flow theory. In all cases the Navier-Stokes Equations were applied with proper boundary conditions and a solution was obtained by assuming that the radius ratio was very large. Without going into detail it is interesting to note some of their remarks about the theoretical

losses. In a bend of 21°, the secondary flow losses were 15% of the total bend losses while in a bend of 90° secondary flow losses were only 1% of the total bend losses.

CHAPTER III

TEST EQUIPMENT

1. Wind Tunnel

Two configurations of the test assembly are shown in Figures 1, 2(a), & 2(b). Figure 1 shows the test elbow followed by a straight duct of a length equal to 4 hydraulic diameters. Figures 2(a) and 2(b) show views of the test assembly when the elbow is connected to the plenum chamber directly.

A family of four 90° bends were tested. Their dimensions are given in the following table:—

	Bend 1	Bend 2	Bend 3	Bend 4
Radius Ratio	1.0	1.0	1.0	1.0
Width	24"	24"	24"	24"
Aspect Ratio	1	3	5	10

The four bends are shown in Figure 3. It is to be noted that for both exit plane configurations the bends were preceded by a straight duct of length 2½ hydraulic diameters.

To insure a flat velocity profile at the inlet of the system a series of contraction cones were used. These contraction cones were designed on the basis of a wall profile given by Smith & Wang (23). In this report use was made of the exact analogy between the magnetic field that is created by coaxial and parallel coils (Helmholtz) carrying an electric current and the velocity field that is created by two ring

13

vortices.. A family of these curves was developed and the theoretical precision of the uniformity of the throat speed for these curves is also given by the authors. Information is provided only for three dimensional axisymmetric nozzles. Using the curves in this report four contraction cones were manufactured, each corresponding to one aspect ratio. The outlet sections of these cones were (1) 24" x 2 4"; A=1, (2) 24" x 8"; A=3, (3) 24" x 4.8"; A=5 and (4) 24" x2.4"; A=10. Since in the present work these sections were rectangular, profiles of the two sides of the bell mouth (containing the 24" side) were designed on the basis of the profiles given by Smith and Wang. Profiles of other two sides were obtained by linear interpolation and full details are given in Appendix I.

The bell mouth was followed by a straight section of duct 8 feet in length. The other end of this section was connected to a straight duct of length 2½ hydraulic diameters which preceded the elbow. The 8 feet length of the duct following the bell mouth was kept the same for all tests. This section helped in developing the flow.

The elbow was followed by a straight duct of length 4 hydraulic diameters and the exit of this straight duct was connected to a 4' x 5' x 4' plenum chamber. To study the effect of discharge conditions on the elbow in later tests, the 4 diameter long duct following the elbow was removed and the elbow connected directly to the plenum chamber. A photograph of this configuration is shown in Figures 2(a) and 2(b). The plenum chamber facilitated the connection of different aspect ratio ducts to the fan and also raised the axis of the assembly. For example the axis of the fan was 32" above the floor whereas the axis of the test section was 48"

above the floor. The plenum chamber was made of 3/4" plywood fastened to an angle iron frame and made airtight with addition of a caulking compound.

To provide for a more efficient operation of the fan a straight section approximately 15½" long, complete with straightening vanes, was fitted between the plenum chamber and the fan. The fan was a Sheldon 19 x Mill Exhauster type. This fan had the capacity to deliver 10,920 cubic feet of air per minute against 6" static head of water at 1,282 rpm and 18.6 B.H.P.

The prime mover was a Greenwood & Batley steam turbine capable of producing 20 H.P. at its maximum output shaft speed of 3,000 rpm. The power was transmitted from the turbine to the fan by a V belt drive having a speed reduction of 2.26:1 which allowed a maximum fan speed of 1,330 rpm. The turbine provided a constant shaft speed which could be held within $\pm$1%. At the outlet of the fan a diffuser of 4' x 4' x 17.5" was fitted to regain some of the pressure losses across the fan.

2. Test section, Instrumentation and Measuring Equipment

The test section consisted of a family of four 90° bends all having radius ratio of unity and a width of 24". Aspect ratios were 1, 3, 5 and 10 for the four bends. These bends were made of plywood by laminating 3/4" plywood sections, having the correct radius of curvature, to build a height of 24". All the straight sections were made of ½" plywood with stiffeners and the contraction cones were made of 1/8" plywood with a wooden frame.

Both the bends and straight sections were fitted with static

pressure taps on the vertical and horizontal walls. Details of the static pressure taps and their locations are shown in Figure 6. The static pressure taps for all stations 0 to 13 were installed using the same pattern. The static pressure taps were made using a mahogany wood button in which was inserted a stainless steel hypodermic tube of .032" O.D. and wall thickness of .008". A brass adaptor 3/16" O.D. was soldered to the outside end of the hypodermic tubing to facilitate making a manometer connection. For the 24" x 24" section 150 such plugs were fitted in the whole system. The installation was made by drilling ½" diameter holes in the wall and these manufactured plugs were carefully glued in position so that they were flush with the inner surface.

The velocity traverses were carried out at 6 stations whose locations are shown in Figure 5. It is to be noted that one of these stations was at 45° plane of the bend. Figure 5 also shows the two traversing planes which were investigated.

The velocity measurements were carried out using a "L" shaped pitot-static probe of conventional design. The tip diameter of the probe was .082". The boundary layer measurements were made using a small scale pitot probe the tip of which had been flattened. Its tip dimensions were .025" x .01" (outer) with a wall thickness of approximately .003". Both of these probes are shown in Figure 4. The turbulence measurements were carried out using a DISA model 55A01 constant temperature hot wire anemometer employing a probe fitted with tungsten wire .0002" in diameter and having a length of approximately .08".

Two types of traversing mechanisms were utilised during the experiment. The coarse traverser, used across the sections, had a range of 14" and advance of 1/20" per revolution. The finer traverser employed a microhead having a range of 1". This later traverser was used for boundary layer measurements and could be set accurately up to .001". Both of these traversers are also shown in Figure 4.

Pressure measurements were made using an ordinary inclined mano-meter having oil of sp. gr. .826. The loss in total pressure across two sections was measured with the help of a micromanometer* which could read accurately up to .001" of water.

---

*Meriam, model 34FB2, 10" of water maximum

CHAPTER IV

THEORETICAL ANALYSIS

Theoretical Pressure Distribution

The theoretical pressure distribution along the inner and outer walls of the elbow was obtained by solving Laplace's equation for the stream function with the proper boundary conditions. The flow in the bend was assumed to be incompressible, two dimensional and potential.

To study the effect of inlet conditions on the pressure distributions in the bend, two cases were investigated. In the first case a uniform velocity distribution was imposed at the inlet and outlet of the bend. In the second case, a straight section of length one equivalent diameter preceded and followed the bend and a uniform velocity distribution was imposed at the inlet and outlet of the straight sections.

Two methods were followed to determine the stream lines.

1. An electrical analogue method.

2. The numerical solution of Laplace's equation by the Relaxation method.

The details of the above two methods are given in the following paragraph. After finding the stream lines in the bend, the velocity at any point in a stream tube could be obtained by the use of the continuity equation treating the fluid as incompressible. Bernoulli's equation was then utilised to determine the static pressure. Further details are given in Appendix 6.

18

A reasonably quick method of finding the position of the stream lines in the bend was by the use of an electrical analogue. Here the bends were cut to scale from an electrically conducting paper (Teldeltos paper) and silver paint was used to mark the inside and outside surface of the bend. An electric potential was then connected across the surface. To simulate a uniform velocity at the inlet and outlet of the bend, a linear variation of voltage was imposed at these two positions. With the aid of an electric probe and Wheatstone bridge (acting as a null indicator) the equipotential lines were easily sketched in. These lines were analogous to the stream lines in potential flow. This simple analogue has two main sources of errors which are sometimes difficult to eliminate.

First of all it was very important to impose a linear potential drop at the inlet and outlet of the bend. This was roughly obtained by dividing the inlet and outlet section in four equal parts and then applying 25%, 50% and 75% of the total voltage across the bend in an incremental manner. The idea was to force the stream lines at inlet and outlet to be equally spaced. However even with the four divisions of both the inlet and outlet sections the stream lines were not equally spaced. The physical size of the Teldeltos paper and the flexibility of the power supply did not allow a further division of the inlet and outlet sections.

A higher accuracy in the determination of stream lines could possibly have been obtained by enlarging the scale of the

bend. However once again the size was limited by the capacity of
the equipment to maintain a constant voltage on the boundaries
because of the large current drain.

Due to the above reasons a numerical relaxation was used
to calculate the stream function with greater precision. A com-
puter program was written for Laplace's equation in a finite
difference form and the problem was solved using an IBM7040 com-
puter. For the case of uniform velocity at the inlet of the bend,
a grid of 29 x 29 points was used. Co-ordinates of bend and
values of the stream function at the boundaries were given as
input data. For example at the inner boundary of the bend $\psi = 0$
while at the outer boundary $\psi = 100$. At the inlet and outlet
section a linear variation of ψ was taken and the values of ψ
were obtained for the points of the grid inside the bend.
Knowing the values of ψ at all points on the grid, constant ψ
lines were drawn by linear interpolation. For the case of the one
equivalent diameter straight duct before and after the bend, a
grid of 43 x 43 point was used. The boundary conditions remained
the same with the exception that a linear variation of ψ at
inlet and outlet of the straight section was programmed. Further
details regarding the computer program are given in Appendix 6.

The variation of the static pressure along the walls of
the bend obtained from the computer program, is plotted in
Figures 7 and 8. The ordinate in both these figures is the dim-
ensionless static pressure $\triangle P/q$ where $\triangle P$ is the difference be-

tween the static pressure at any point and the static pressure at the entrance to the bend. The q is the free stream dynamic pressure based on the entrance velocity. The abscissa is a dimensionless distance, measured along either the inside or outside wall, divided by the hydraulic diameter. In Figure 8 the length is measured along the mid bend radius and this is why the L/D for the outside and inside wall is the same.

The curves in Figure 7 and 8 are only for a R/d = 1 and it should be noted that height of the peaks will be increased for a smaller value of R/d and will be decreased for a higher value of R/d. The computer program could easily have been modified to obtain the curves for other values of R/d as required. The pressure distributions indicate that at the inner wall there is an acceleration followed by an expansion of the flow, whereas at the outer wall the expansion is followed by an acceleration. The following points are also worth noting of the cases studied:-

1. The maximum and minimum values of $\Delta P/q$ are the same in both cases.

2. The introduction of a straight duct before the bend made the variation of pressure more gradual.

3. The effect of the straight section on the bend is shown only in the region of approximately 15° from the inlet and exit of the bend. The stream function in the remainder of the bend was not noticeably affected by the presence of the straight sections.

A comparison with the experimental results will be made in a later section of the report.

CHAPTER V

EXPERIMENTAL PROCEDURE

This section describes briefly the experimental methods followed in testing the four elbows. The first configuration tested employed the 24" x 24" elbow corresponding to an aspect ratio of I.0. The experimental set up is shown in Figure 1. Four turbine speeds were selected based on preliminary tests. There were (1) 2100 rpm (2) 1775 rpm (3) 1250 rpm and (4) 700 rpm which corresponded to free stream centre line velocities of 42.4, 35.5, 25.0 and 14.4 ft/sec respectively. This selection of the speeds provided Reynolds numbers based on the volume flow rate and hydraulic diameter from 1.7×10^5 to 5×10^5. The measurements taken are described in the following paragraphs.

1. Velocity Traverses

Complete velocity traverses were obtained at station O in both the horizontal and vertical directions for all four turbine speeds. Velocities away from the wall were measured with a standard "L" shaped pitot static probe used in conjunction with the coarse traversing device while velocities close to the wall were measured using the flattened boundary layer probe with micrometer adjustment. With the aid of these profiles the discharge was calculated corresponding to each speed. (Sample calculations are shown in Appendix 3). The main object of these tests was to calibrate the volume flow rate of the

tunnel in terms of turbine speed.

The growth of the boundary layer at the inside wall was studied by taking boundary layer traverses at station 1 for three turbine speeds 2100, 1775 and 1250 rpm. The information obtained from these profiles helped in assessing the flow condition at the entrance to the bend. The technique used to establish the position of the probe with respect to the wall was quite simple. A small section of aluminum foil was cemented to the wall underneath the probe mouth. A resistance meter was then used to detect the contact between the probe and the wall and the traverse was then started in an outward direction.

To investigate the change in the velocity profile, in both the horizontal and vertical directions, as the flow passed from station 0 to 13, one turbine speed (2100 rpm) was selected and velocity traverses were carried out at all stations. Figure 14 shows clearly how the horizontal velocity profile changed as the flow passed through the test configuration. Figure 15 on the other hand shows that there is no appreciable change in the vertical profile throughout the section. A more detailed investigation of the velocity profiles at the 45° radial line (station 6) was obtained by including boundary layer measurements on both the inside and outside walls. These are shown in Figures 21 and 22.

To have a complete picture of the flow in the bend one would like to know at least two of the three quantities static pressure, total pressure and/or velocity profile. Since in any situation where the stream lines have unknown curvature the static pressure is not

very easy to measure for example at stations 1 and 6, a total pressure traverse was taken. Figures 23 and 24 show the horizontal total pressure distribution across these sections.

2. Static Pressure Distribution

The static pressures at the walls of both ducts and elbow were measured at three turbine speeds 2100, 1775 and 1250 rpm with the help of an inclined manometer using oil of specific gravity .826 as the manometer fluid. Twelve readings were taken at each station as described in Figure 6. It was observed that the static pressures were reasonably constant across the sections until station 3 was reached. After this point in the flow the inside wall taps indicated much lower pressures than the outside wall taps. The pressure distributions as shown in Figure 9 were obtained from the pressure taps located at the mid plane of each station. In order to study the effect of discharge conditions on the static pressure distribution a duct of 4 D equivalent length following the elbow was removed and the elbow was allowed to discharge directly into the plenum chamber. Figure 10 shows the pressure distribution curves superimposed for both the above discharge conditions.

3. Turbulence Level

Turbulence measurements were considered necessary to define as completely as possible the flow entering the bend. The turbulence level at three Reynolds numbers was measured in the horizontal plane

only at station 0 and is shown in Figure 26 . The free stream tur-
bulence level was found to be approximately 1.6%.

4. <u>Total Pressure Measurements</u>

Total pressure surveys were carried out upstream and down-
stream of the test section in order to determine the total pressure
loss across the elbow. These measurements were made for the two test
configurations in which the elbow was first of all discharged to a
constant area duct and secondly connected directly to the plenum
chamber.

(1) Elbow discharging to the plenum chamber through a 4D
length duct.

Preliminary tests showed that the loss in the total pressure
across the elbow could not be measured directly by taking the dif-
ference in total pressure before and after the elbow, because the
flow after the elbow was quite distorted and the stream direction was
not clearly defined. It was found more convenient and accurate to
measure the total pressure loss between station 3 and 13. The loss
due to the discharge duct of 4D length was then subtracted from the
above loss to obtain the loss in total pressure across the elbow. Two
stagnation probes were mounted at station 3 and 13 in the same relative
position and were connected to a differential manometer. The loss in
total pressure was obtained using a micromanometer as a pressure dif-
ferential measuring device. Traverses were carried out on all four

walls to complete the pressure survey. Figure 27 shows some typical curves obtained of the loss in total pressure across the section.

(2) Elbow discharging to the plenum chamber directly.

For the test configuration in which the elbow was mounted directly on the plenum chamber two types of measurements could be made. These concerned both the static pressure and total pressure since if the plenum chamber is large compared to the duct the velocity in the chamber can be considered small and therefore the total pressure and static pressure can be taken as equal. The total and static pressure readings were taken at station 3, and then knowing the average pressure of the plenum chamber, both the above losses were computed and are presented in Figure 29.

For tests on the elbows of aspect ratios 3, 5 and 10, the turbine speed was adjusted in such a manner as to give nearly the same Reynolds number used in the tests for an aspect ratio of 1.0. For an aspect ratio of 3, a complete velocity traverse was carried out at station 0 to calculate the discharge. However, it was found that in testing elbows of aspect ratios 5 and 10 the velocities in the test section became quite high and it was not considered necessary to carry out complete boundary layer surveys to calculate the discharge.

After calibrating the tunnel for aspect ratios of 3, 5 and 10, the loss in total pressure was measured using the same technique as employed for aspect ratio 1.0.

Static pressure distribution and turbulence measurements were not carried out for the last three aspect ratios because of lack of time and it was assumed that their trends would remain essentially the same. By eliminating some of these measurements the number of static pressure taps was considerably reduced. For example with the higher aspect ratio bends only 4 pressure taps were installed at each station instead of 12 and no pressure taps were placed in the bend.

It was interesting to note that when the elbow was discharging directly to the plenum chamber the turbine speed had to be increased above the speed in the case of the elbow discharging through a constant area duct for the same Reynolds number. This indicated a higher loss in the former case.

Because of the necessity of determining a value of ϵ/D for the straight duct used in the experiment, the centre line loss in total pressure was also measured between stations 0 and 1. This enabled one to calculate a suitable friction factor for use with the straight duct.

CHAPTER VI

ANALYSIS OF DATA

1. Computation and Presentation of the Data

Because of the large number of experimental readings taken during the tests, mainly pressure measurements, it was considered most appropriate to present the results in a graphical form. Some computations were required in the reduction of the readings but these were in general straight forward. For example the velocities were calculated from the readings of the dynamic head in inches of water using the standard Bernoulli's formula assuming the working fluid (air) to be incompressible and having a static temperature of 70°F. The maximum velocity achieved in the highest aspect ratio bend was of the order of 136 ft./sec. and is well within the limits of the assumption of incompressible flow.

The boundary layer traverses carried out on the centre line of the four sides of the duct enabled one to calculate the displacement thickness using the standard incompressible form:-

$$\delta^* = \int_0^\delta (1 - \frac{\bar{u}}{\bar{V}}) \, dy$$

The displacement thickness calculated at the centre of the wall was assumed to be constant at all points on the wall at station 0. With this assumption and having an average value of δ^* the effective area was calculated in which velocity could be assumed

constant. The volume flow rate was then calculated and finally the Reynolds number was determined based upon the hydraulic diameter and mean velocity. A sample calculation is shown in Appendix 3.

Boundary layer profiles are also presented in logarithmic form in Figure 20 for station 1 which lies at the exit of 8 ft. long duct following the contraction cone. These profiles were useful in determining the condition of the working fluid at the entrance to the bend.

The static pressure distributions along the walls of the bend at midheight are presented in Figures 9 and 10 in a dimensionless form. In order to compare these experimental curves with the theoretical results presented in Figures 7 and 8, they have been plotted in the same fashion as indicated in Chapter IV. In Figure 10 the average plenum chamber static pressure divided by q of the free stream before the bend provides the dimensionless dump pressure.

The static pressure variation along the 45° radial line at midbend height is shown in Figure 25. The inner and outer wall static pressures at the 45° radial line in Figure 25 are the same as those given in Figure 9. Static pressures in the boundary layer and free stream have been calculated with the aid of Figure 24 and Figures 13 and 15. In Figure 24 the total pressure variation is shown while Figures 13 and 14 give the variation of the velocity head across the section. Their difference presented in

Figure 25 is the static pressure.

Figure 27 shows typical curves for the total pressure loss variation across the section 24" x 24" between station 3 and 13. No attempt was made to take the total pressure readings very close to the wall because they had very little effect on the integrated result. Each of these curves was graphically integrated across the section and the mean effective loss in total pressure, which was equal to ratio of the area under loss curve to the length of the traverse, was calculated.

Having calculated the mean effective loss in total pressure for the horizontal and vertical traverses at each Reynolds number, an arithmetic average was obtained. From the centre line measured loss in total pressure between station 0 and 1, a Moody friction factor was calculated. This provided a value of ϵ/D for the duct since the Reynolds number was also known. The experimental measurement of the loss in total pressure in the duct also allowed one to calculate the loss in total pressure across the elbow since the elemental loss could be easily subtracted from the arithmetic average.

This indirect method of determining the loss across the elbow was employed because, due to the disturbed flow in the bend, it was not possible to measure the total pressure at the exit of the bend with any degree of accuracy. The loss in total pressure across the elbows is presented in Figure 28 (a, b, c, d).

Figure 29 provides curves showing the total and static pressure loss coefficient as a function of aspect ratio when the elbow is discharging directly to the plenum chamber. The following formulas were used in calculation of the loss coefficients:-

$$\frac{\triangle P_{static}}{q} = \frac{\text{Average plenum chamber pressure} - (P_{static})_{station\ 3}}{q}$$

$$\frac{\triangle P_{total}}{q} = \frac{\text{Average plenum chamber pressure} - (P_{total})_{station\ 3}}{q}$$

The turbulence levels shown in Figure 26 were obtained by taking readings of E_{rms}, E (d. c. voltage) and E_o (bridge voltage at 0 velocity) and employing the following formula:-

$$\% \text{ turbulence} = \frac{u'}{u} \times 100 = 100\ E_{rms} \times 4E/(E^2 - E_o^2)$$

For the derivation of this formula see Appendix 2.

The position of the maxima in Figure 26 is not very accurately known as it was quite difficult to find out exactly when the hot wire probe touched the wall. In Figure 26 (top), two points are shown corresponding to each reading. These indicate the maximum and minimum

readings obtained. The solid and dotted lines represent the mean curves between the two limits.

2. Error Analysis

The errors in the measurements of both pressure and turbulence are mainly due to the fluctuations in the flow. A table for the probable error is given below. The actual error is always smaller than that given in the table which is based upon worst possible combination of individual errors.

Quantity	Maximum error
Duct wall static pressure	$\pm$ 4%
Pitot static probe (in straight duct)	$\pm$ 2%
Pitot static probe (in elbow)	$\pm$ 6%
Total pressure loss across elbow	$\pm$ 10%
Average plenum chamber static pressure (excluding 24" x 24" section)	$\pm$ 15%
Percentage turbulence (away from the wall)	$\pm$ 30%
Percentage turbulence (near the wall)	$\pm$ 2%
Distance of boundary layer probe from wall	$\pm$ .0005"
Speed of turbine	$\pm$ 1%
q ($\frac{1}{2} \rho V_{av.}^2$)	$\pm$ 2%
$\triangle P_{static}/q$	$\pm$ 6%
ρ	$\pm$ 1%
μ	$\pm$ 1%
Volume flow rate	$\pm$ 3%
Reynolds number	$\pm$ 5%
Power law velocity exponent	$\pm$ 10%

CHAPTER VII

DISCUSSION

For the sake of convenience, this chapter has been divided into two parts. The first part is a discussion on pressure distribution, velocity profile and turbulence. The pressure loss measurements are discussed in the second part.

1. Pressure Distributions, Velocity Profiles and Turbulence

The side wall pressure distributions as shown in the Figure 9 and 10 have been obtained from readings of pressure taps no. 5 and 11 for each successive section. These taps are located at the mid plane height of the inside and outside walls respectively. As the flow turns around the bend, the inside wall pressure taps indicate a lower pressure than the corresponding outside wall taps. Pressure tap no. 2 and 8 however, located at the middle of top and bottom wall show no appreciable change in the pressure reading up to station 8 which is at the exit of the bend. The pressure reading given by tap 6 appears to lie between the two adjacent taps 5 and 7. The same thing is true for taps no. 4, 10 and 12 which have the same relative position as the tap no. 6. At station no. 12, which is one hydraulic length upstream of the plenum chamber, all the taps indicate nearly the same static pressure although the inner wall was still showing a slightly lower pressure compared to the outer wall. The static pressure at station 13, which is situated at the exit of 4 D long constant

area section following the bend, was found to be lower than the
static pressure before the bend (station 3). This effect appears in
Figure 9 and 10 as a finite value of $\triangle P/q$ at station 13. This, in
actual fact, represents the loss in static pressure. When the elbow
is discharging directly to the plenum chamber, one can see this effect
more clearly, as the loss in static pressure increases considerably
with the latter configuration.

It is worthwhile comparing the experimental pressure dis-
tribution around the bend with the theoretical distribution given in
Chapter 4. This comparison is shown in Figure 9. The theoretical
pressure distribution on the outside wall agrees well with the
experimental curve. The maximum value of $\triangle P/q$ on the inside wall
as given by theoretical curve is - 1.56 compared to a value of - 2.0
given by experimental results. Similarly the maximum value of $\triangle P/q$
at the outside wall as given by the theoretical curve is + .53 whereas
the experimental value is + .50. It can be seen that the agreement
between the two curves is better for the first 45° segment of the bend
than the last 45° segment. The reason for this discrepancy is the
adverse pressure gradient which causes the flow separation on the
latter section of the inside wall. At this point, it is worthwhile
comparing the curves given by "Higginbotham, Woods and Valentine"(7)
with the present results. Their theoretical value for the maximum
$\triangle P/q$ on the inside wall is - 1.0 and the maximum $\triangle P/q$ on the
outside wall is + .50. Their experimental value however for the
inside wall is given as - 2.0 while the outside wall value remains
at + .50.

The agreement between the experimental results given in
Figure 9 for the present work and Reference 7 is very good. The only
discrepancy is in theoretical value of $\triangle$ P/q at the inside wall. The
authors of Reference 7 have failed to mention the inlet and outlet con-
ditions of the flow which they have imposed for the relaxation solution.
Since the pressure distribution depends upon the inlet and outlet con-
ditions of the flow, it may possibly account for the difference in
the values of $\triangle$ P/q obtained on the inside wall.

Figures 11 and 12 describe the general pattern of the air velocities
after it has passed through the contraction cone. Figure 11 for
example shows that the velocities in the vertical plane are quite
symmetrical. The velocities in the horizontal plane, taken at mid
plane height, show a slightly different growth of the boundary layer
comparing the inside and outside walls. The contraction cone design
appears to give quite uniform velocity distributions in the exit plane.
Figure 12 shows typical velocity distributions for aspect ratios of
3, 5 and 10. As in the case of aspect ratio one, the contraction cones
appear to provide a high degree of uniform flow. However an analysis of
the boundary layer growth in the duct shows some differences comparing
the four walls. It was also observed that the contraction cones designed
for high aspect ratios deformed slightly at the maximum Reynolds number.
No boundary layer measurements were carried out for the tests on the
elbows having an aspect ratio of 5 and 10 since the velocity markedly
increased in the system and this considerably reduced the displacement
thickness at the exit plane of the contraction cone where the volume

flow rate was measured. It was felt that neglecting the displacement

thickness for the higher aspect ratio would not seriously affect the

calculation of the volume rate and therefore the Reynolds number.

The velocity traverses indicated that for 24" x 24" section,

an 8 feet length of the duct downstream of the bell-mouth was not

enough to develop the flow although it did provide a stabilizing effect.

Measurements taken on the inside wall at stations O and 1 show that the

δ^* (displacement thickness) was 0.137" & 0.215" respectively for a

Reynolds number of 4.75 x 10^5. Figure 20 shows that the value of "n"

obtained from a log plot of the power law, is between 5 and 6 and hence

the boundary layer is fully turbulent. An attempt was made to fit the

power law velocity profile to the boundary layer measurements taken

at station O but the agreement was poor since the flow was still

accelerating from the bell-mouth.

As the flow turns around the bend, the velocity at the inside wall

increases, whereas the velocity at the outside wall decreases. Figure

14 shows this effect quite well. The flow after turning 90° has

apparently separated from the inner wall and occupied the outer portion

of 4D length duct following the bend. The velocity traverses taken at

station 13 (Figure 14) show this point very well: in this diagram

the velocity at the inner wall is small compared to that at the outer

wall. The vertical traverse at station 13, which is shown in Figure

15, possibly represents some effect of the plenum chamber. It can be

seen that there is a pronounced dip in the velocity profile at the

centre although there is a reasonable degree of symmetry. It was

found that as the aspect ratio increased this effect became more pronounced. Some effect of the secondary flow was also noticed.

A curve of the turbulence level as a function of horizontal distance is shown for three Reynolds numbers in Figure 26. These measurements were all made at station O. The turbulence level in the centre of the duct is of the order of 1.6% and was found to increase very sharply near the wall. The general trend of the curves is in agreement with the results given by Lauffer (24). It is to be noted that the level of the turbulence is higher for the smaller Reynolds numbers. Lauffer in his report, has pointed out that $\sqrt{\overline{u'}^2}/\overline{u}$ reaches a maxima within the laminar sublayer ($yV^*/\nu \approx 17$) and that it tends towards a constant value of 0.18, at the wall, which is independent of the Reynolds number. For the present work it was not considered necessary to obtain accurate turbulence measurements near the wall and with the present experimental set up it was difficult to determine the position of maximum turbulence very accurately. It was however noted that the fluctuation in the readings of $\sqrt{\overline{u'}^2}$ near the wall was very small compared to those taken in the free stream. For example, at a Reynolds number 2.9 x 10^5 the turbulence level near the wall was 39% to 41% whereas at 3" from the wall it was between 3% and 6%.

2. Pressure Loss Measurements

A typical total pressure loss curve obtained from horizontal and vertical traverses is shown in Figure 27. The horizontal traverse shows that there is more loss in the inside half portion of the duct

when compared to the outer half portion of the duct. This trend was noticed in the results for four aspect ratios. A look at the horizontal velocity traverse at station 13 and 3 (Figure 14) will help to explain why this type of curve is obtained. The velocity profile at station 3 is flat and hence the total pressure at 3 is nearly constant throughout the section. But the velocity at station 13 in the outer portion of the duct is higher than it is in the inner portion. This indicates a higher total pressure in the outer portion as compared to the inner region. Hence the loss in the outer portion of the duct is less than that in the inner portion.

In a similar manner the vertical traverse of the total pressure loss curve shows more loss in the central portion of the duct than near the wall. The vertical velocity traverse at station 13 (Figure 15) indicates a depression in the centre. Thus the central portion represents a lower total pressure in the section provided that the static pressure across the section remained essentially constant. This effect is possibly due to the presence of the plenum chamber, otherwise one would expect a flat curve. For higher aspect ratios (A=3, 5 and 10), the effect of the secondary flow also comes into picture and this, combined with the presence of plenum chamber, modifies the total pressure loss curve in the vertical direction.

It is to be noted that total pressure loss, which was measured between station 3 and 13, shows a negative value (which means increase in total pressure) near the outside wall of the duct. This negative value is obtained due to difference in growth of the boundary layer between station 3 and 13. Since the velocity at station 13 on the

outside wall is higher than at station 3 on the outside wall, it
suggests that the boundary layer thickness on the outside wall at
station 13 is smaller when compared to station 3. Because of this
difference in growth, at the same geometric distance from the wall,
there may be gain in the total pressure. To be exact one should
examine the difference in the total pressure between points which lie
on the same stream line, because only then would it be correct to say
that a particle of air while travelling from station 3 to station 13
undergoes a loss in total pressure. Since this is not very practicable,
one has to assume that the stream lines are parallel to the walls and
points which are at equal distance from the wall correspond roughly to
the points on the same stream line.

In Figure 28 (a, b, c, d) experimental points obtained from the
integration of curves in Figure 27 are superimposed upon the curves
taken from Reference 10 and 22. At present these are probably the most
widely accepted total pressure loss curves. As has been mentioned
previously a review of the work in Reference 22 shows that these curves
are not totally experimental but because of the large number of possible
configurations involved, some interpolation has been done. The author
in Reference 22 has taken these curves from NACA ARR L4F26(4), but in
Reference 4 curves are only given for three Reynolds numbers 1×10^5,
3×10^5 and 6×10^5 whereas in Reference 22 curves for 1×10^5, 2×10^5,
3×10^5, 4×10^5, 5×10^5 and 6×10^5 Reynolds number are presented
which clearly shows that interpolation has been carried out. In
Reference 4 the author has mentioned that the curves are based on
References 2, 6, 18, 19, 20 and 21.

A comparison of the present experimental results with the curves given in Ref. 22 confirms qualitatively the trend of the curves for low aspect ratios but shows considerable deviation as the aspect ratio became very high. Figure 28 (a) and 28 (b), for example, for aspect ratios of 1 and 3 respectively, show reasonable agreement with the original results. The measured loss coefficients are on the average higher than the curves predict by some 27%. The inlet conditions to the present tests cannot be compared to original results and it is quite possible that the curves in fact do shift vertically for thin boundary layer entrance conditions. There is also a lack of uniformity on the method of measuring the total pressure loss across the bend and further confirmation and agreement need to be reached in these areas.

Shown also for comparison is a curve given by the experimental results of Ito (9) as presented by Smith (10). These results were obtained in circular cross section pipe bends of the same radius ratio (1.0) in which the flow was fully developed. The static pressure measurements were taken across the bend by manifolding the static pressure taps downstream of the bend to provide an average value. This technique, admittedly useful for many applications, has some drawbacks where one considers the static pressure variation which occurs across the exit plane of the bend.

Figure 28 (b), describing the results obtained for an aspect ratio of 3.0, also shows a trend consistent with those supplied by Reference 22 although once again the present experimental results are higher by approximately 30%.

The most notable differences in the present results with those of Reference 22 are shown in Figure 28 (c) and 28 (d). In Figure 28 (c) the trend of the experimental results is considerably different than that of the curves presented. The trend of the experimental results does agree with those obtained at lower aspect ratios although it could be argued that in the vicinity of aspect ratio 3.0 a reversal in the shape of the curves might take place. Once again the inlet conditions which affect the bend performance should be fully specified before any proper comparison can be made. It may in fact be entirely out of place to compare the present results with those given in Reference 22. However the comparison has been made to lend further weight to the conclusions that the inlet and exit plane conditions seriously affect the bend performance.

The present experimental setup allowed only two tests to be carried out on the bend having an aspect ratio of 10, and at the same time stay within the required Reynolds number range. The results of these two tests are shown in Figure 28 (d) and stress the need of further experimental work in this area.

Measurements of the loss in total pressure for the straight portion of the duct (8' long) give results which lie slightly above the smooth pipe curve given in the Moody Diagram*. These measurements suggest that the valve of ϵ for the duct should lie between .00005 and .0001 feet. Friction factor measurements are given in Appendix 4.

---

* "Handbook of Fluid Dynamics" by V. L. Streeter Page 3 - 12

The effect of exit plane conditions on the loss coefficient was also studied. The total pressure loss and static pressure loss are shown in Figure 29 for the case when the elbow is discharging directly to the plenum chamber. The pressure losses are based upon average static pressure in the plenum chamber. Some difficulty was encountered in measuring the average static pressure in the plenum chamber. Ten static pressure taps in the walls of the plenum chamber showed some variation in static pressure, especially for the case of aspect ratio 1 (24" x 24" duct). In this case the plenum chamber was not large enough to maintain a constant static pressure at the outlet section. It is worthwhile noting that the inside wall of the plenum chamber was at somewhat lower static pressure than the outside wall which means that the effect of the bend was felt in the plenum chamber also. However at the higher aspect ratios as the volume flows became smaller the scatter in the static pressure readings in the plenum chamber were reduced. For example at a Reynolds number of 2.9×10^5 the static pressure in the plenum chamber was $0.242 \; {}^{+\; 24\%}_{-\; 4\%}$ and $2.13 \pm 6\%$ inches of water at an aspect ratio of 1.0 and 5.0 respectively. Because of this effect, a band has been included in Figure 29 which covers most of the experimental points. With the information at hand one is not able to effectively correlate the measured loss coefficient with Reynolds number. It should also be noted that for an aspect ratio of 10.0 only two readings are available in the desired Reynolds number range. This is due to the fact that at the higher Reynolds numbers one reaches the limitation of the static pressure head provided by the fan.

CHAPTER VIII

CONCLUSIONS & RECOMMENDATIONS

A number of interesting conclusions can be drawn regarding
the measured pressure loss coefficient. The present experimental
results confirm qualitatively the trend of the curves given in
NACA L4F26 (4) for lower aspect ratios. In general at lower aspect
ratios the experimental points give the total pressure loss coefficient
which is approximately 25% higher than those given by the NACA report.
At higher aspect ratios the experimental points do not agree with the
curves given in the NACA report. Since the inlet and exit conditions
affect the bend performance, the comparison may not be justified. When
the elbow discharged through a duct of length 4 hydraulic diameters,
the total pressure loss coefficient was of the order of 0.25. The
removal of the discharge duct increased the total pressure loss
coefficient by approximately 5 to 6 times.

From the theoretical and experimental pressure distribution
obtained around the walls of the bend, it can be concluded that the
flow is more potential on the outside wall of the bend than on the
inside wall. The turbulence level measurements were in agreement with
the earlier workers in the field. In the centre of the duct the turbulence
level was of the order of 1.6%

The velocity measurements were quite helpful in visualizing
the various flow regimes. These measurements indicated that the flow
before entering the bend was not fully developed but that the boundary
layer on the walls was turbulent.

The size of the duct used in the experiment is similar to those used in ventilation and heating work. Hence the results can be directly applied without any significant error due to the scale effect. The larger size of the duct, however, does introduce some problem in achieving higher Reynolds number due to large mass flow required. Also the larger duct size poses a further problem because of the increasing length of the duct necessary to obtain any significant change in the inlet flow profile.

The accuracy in the measured loss coefficient, when the elbow is directly discharging to the plenum chamber can be improved if a blower is used instead of a fan. The use of the blower will eliminate static pressure measurements at the exit since the elbow can discharge directly to the atmosphere. However, entrance conditions are difficult to manage with a blower installation as it requires a well designed settling chamber.

It was noticed that even after a 4 D length downstream of the elbow, the flow was quite disturbed. This suggests that a simplification in the measurements of the loss in total pressure and thus higher accuracy in the results can be obtained if the length of the discharge duct is increased. To achieve this with the present experimental set up, one would have to work with smaller hydraulic diameter ducts and therefore a reduction in the Reynolds number. On the other hand, the discharge duct cannot be made too long because in the deduction method to obtain the loss due to the elbow one has to subtract the friction loss in the straight duct from the combined loss across both the elbow

and duct and it can be seen that if the duct is too long both these losses become of the same order and their subtraction will decrease the accuracy of the results. For future work it is recommended that the discharge duct of a length between 8 and 12 hydraulic diameters would give more consistent results.

CHAPTER IX

NOMENCLATURE

Symbols	Description	Units
a	Cross-sectional area	$in.^2$
d	Depth of bend (see Fig. 16)	in.
D	Hydraulic diameter	in.
E	D.C. voltage in hot wire	volts
E_{rms}	R.M.S. voltage in hot wire	volts
E_o	D.C. voltage corresponding to zero velocity	volts
F	Meaning function of	–
f	friction factor	–
L	Length along wall	ft.
n	Power law exponent	–
$\triangle P_{total}$	Loss in total pressure	$lbf/ft.^2$
$\triangle P_{static}$	Loss in static pressure	"
q	Dynamic head $(1/2 \, \rho \, V_{av.}^2)$	"
r	Radius of curvature at any point	ft.
R	Radius of curvature at mid bend surface	ft.
r_c	Radius of curvature at inner bend surface	ft.
r_o	Radius of curvature at outer bend surface	ft.
$\bar{u}$	Mean local velocity	ft./sec.
$\sqrt{\overline{u'^2}}$	R.M.S. fluctuating velocity in direction of $\bar{u}$	ft./sec.
w	Width of bend (see Fig. 16)	in.
v^*	Friction velocity	ft./sec.
Vav.	Average velocity over section	ft./sec.

Nomenclature (continued)

Symbols	Description	Units
V	Centre line velocity at any section	ft./sec.
y	distance measured away from wall	in.
δ	Boundary layer thickness	in.
δ^*	Displacement thickness	in.
ρ	Density	$lb_m/ft.^3$
ψ	Stream function	$ft.^2/sec.$
ν	Kinematic viscosity	$ft.^2/sec.$
ϵ	Surface roughness	ft.
μ	Dynamic viscosity	lb/ft.sec.

Dimensionless

Parameters

A	Aspect ratio w/d
RR	Radius ratio R/d
Re	Reynolds number $\rho VavD/\mu$
K	Total Pressure loss coefficient $\Delta P_{total}/q$
u/v^*	Universal velocity distribution parameter
yv^*/ν	Universal velocity distribution wall distance parameter

CHAPTER X

REFERENCES

1. Busey, F.L.: Loss of pressure due to elbows in the transmission of air through pipes or ducts. Trans. of American Society of Heating & Ventilating Engineers, Volume 19, 1913, page 366.

2. Wirt, Loring: New data for the design of elbows in duct systems. General Electric Review, Volume 30, No. 6, June 1927, pages 286-296.

3. Madison, R.D. & Parker, J.R.: Pressure losses in rectangular elbows. Trans. ASME, Volume 58, 1936, pages 167-176.

4. Henry, J.R.: Design of power plant installations-Pressure loss characteristics of duct components. NACA ARR No. L4F26, 1944.

5. Weske, J.R.: Investigations of the flow in curved ducts at large Reynolds Number. Journal of Applied Mechanics, December 1948, pages 344-348.

6. Weske, J.R.: Pressure loss in ducts with compound elbows. NACA WRW-39, February 1943.

7. Higginbotham, Wood & Valentine: A study of high speed performance characteristics of 90 degree bends in circular ducts. NACA TN 3696., 1956.

8. Ito, H.: Friction factor for turbulent flow in curved pipes. Journal of Basic Engineering, June 1959, page 125.

9. Ito, H.: Pressure losses in smooth bend pipe. Journal of Basic Engineering, ASME Trans., V-82, Ser D, March 1960.

10. Smith, A.J.W.: The flow and pressure losses in smooth pipe bends of constant cross section. Journal of The Royal Aeronautical Society, Volume 67, July 1963, pages 437-447.

11. Wattendorf, F.L.: A study of effect of curvature on fully developed turbulent flow. Proceedings of Royal Society of London, Series A, Volume 148, February 1934.

12. Weske, J.R.: Experimental investigation of velocity distribution down stream of single duct bends. NACA TN 1471, 1948.

13. Eskinazi, S.: An investigation of fully developed turbulent flow in curved channel. John Hopkins University Contract number Non r 248(33), August 1954.

14. Yeh, H.: Further investigations on fully developed flow in curved channels. John Hopkins DSIS (57/03227) 856, 1956.

15. Hawthorne, W.R.: Secondary circulation in fluid flow. Proc. of Roy. Soc. of London, A, Volume 206, 1951, page 374.

16. Detra, R.W.: Secondary flow in curved pipes. Mitteilungen aus dem Institut fur Aerodynamik E.T.H. Zurich Nr. 20, 1953.

17. Eichenberger, H.P.: Shear flow in bends. Office of Naval research, Contract No. 5, Orgi 07848, Tech. Report No. 2, 1952.

18. Patterson, G.N.: Note on the design of corners in duct systems. R. & M. No. 1773, British A.R.C., 1931.

19. Patterson, G.N.: Corner losses in ducts. Aircraft Engineering Volume IX, No. 102, August 1937, pages 205-208.

20. Abramovich, G.: Fluid motion in curved channels. From collection of reports on Industrial Aerodynamics and Fan construction report No. 211 (text in Russian), Trans. Central Aerodyn. Inst. (Moscow), 1935, Pages 97-151.

21. McLellan, Charles H., Bartlett, Walter A., Jr.: Investigation of air flow in right angle elbows in a rectangular duct. NACA ARR October 1941.

22. SAE Aeronautical information report number 23, October 15, 1951.

23. Wade, J.H.T.: Contraction cones giving uniform throat speeds (A literature survey), Orenda Aero Note 185, May 1956.

24. Lauffer, J.: Investigation of turbulent flow in a two dimensional channel. NACA Report 1053, 1951.

25. Preston, J.H.: The determination of turbulent skin friction by means of pitot tubes. Journal of the Royal Aeronautical Society, Volume 58, February 1954, pages 109-121.

26. Aero-Space Applied Thermodynamics Manual, Published by Society of Automotive Engineers, Inc., Committee A-9 Aerospace environmental systems, February 1960.

CHAPTER XI

ILLUSTRATIONS

FIG. NO.1

LAYOUT OF TEST FACILITY SHOWING
24" x 24" ELBOW DISCHARGING TO
PLENUM CHAMBER THROUGH 4 D LONG DUCT

NUMBERS 0 TO 13 SHOW THE POSITION
OF STATIC PRESSURE STATIONS
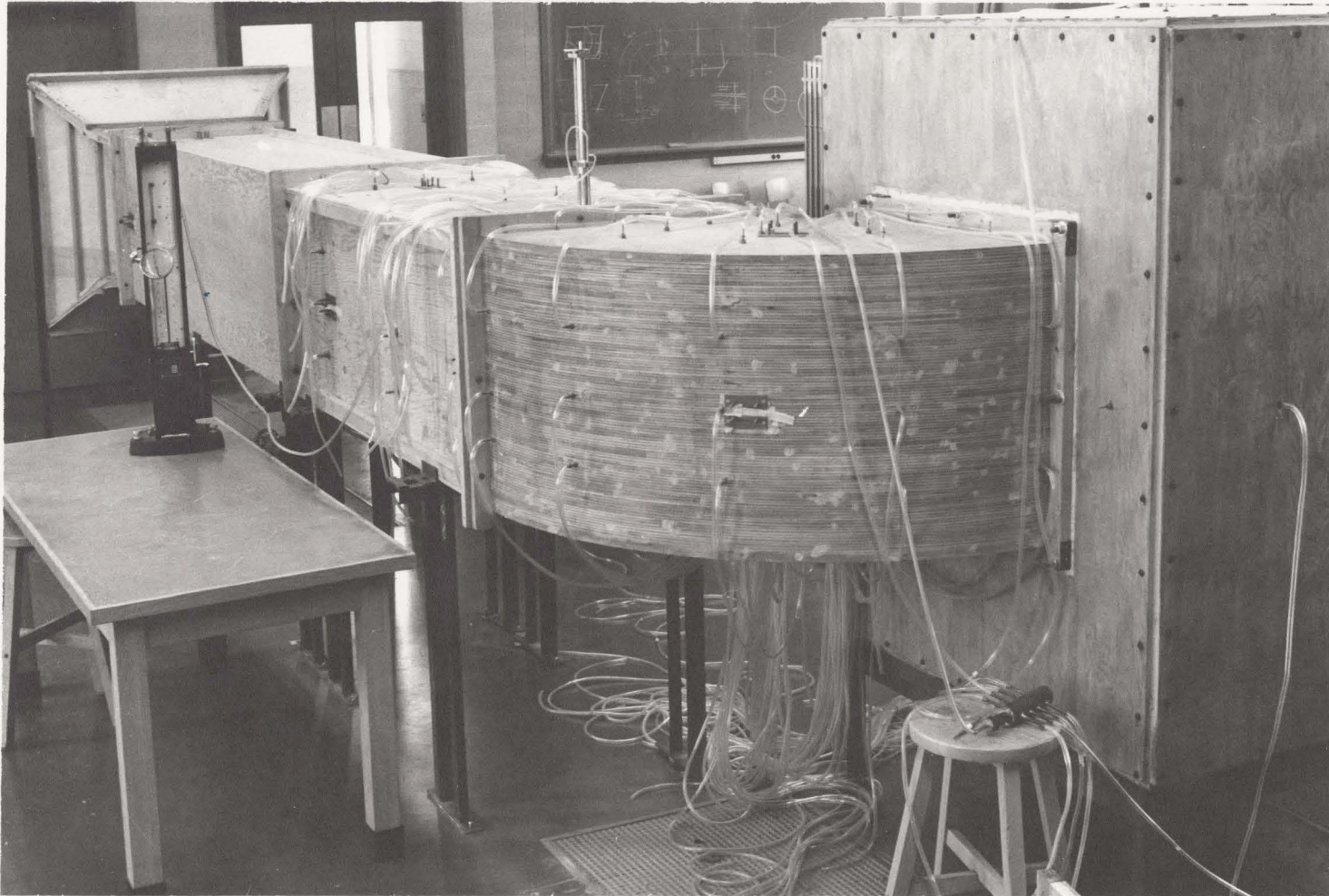
FIGURE 2 (a)

TEST FACILITY - ELBOW DISCHARGING TO PLENUM CHAMBER DIRECTLY
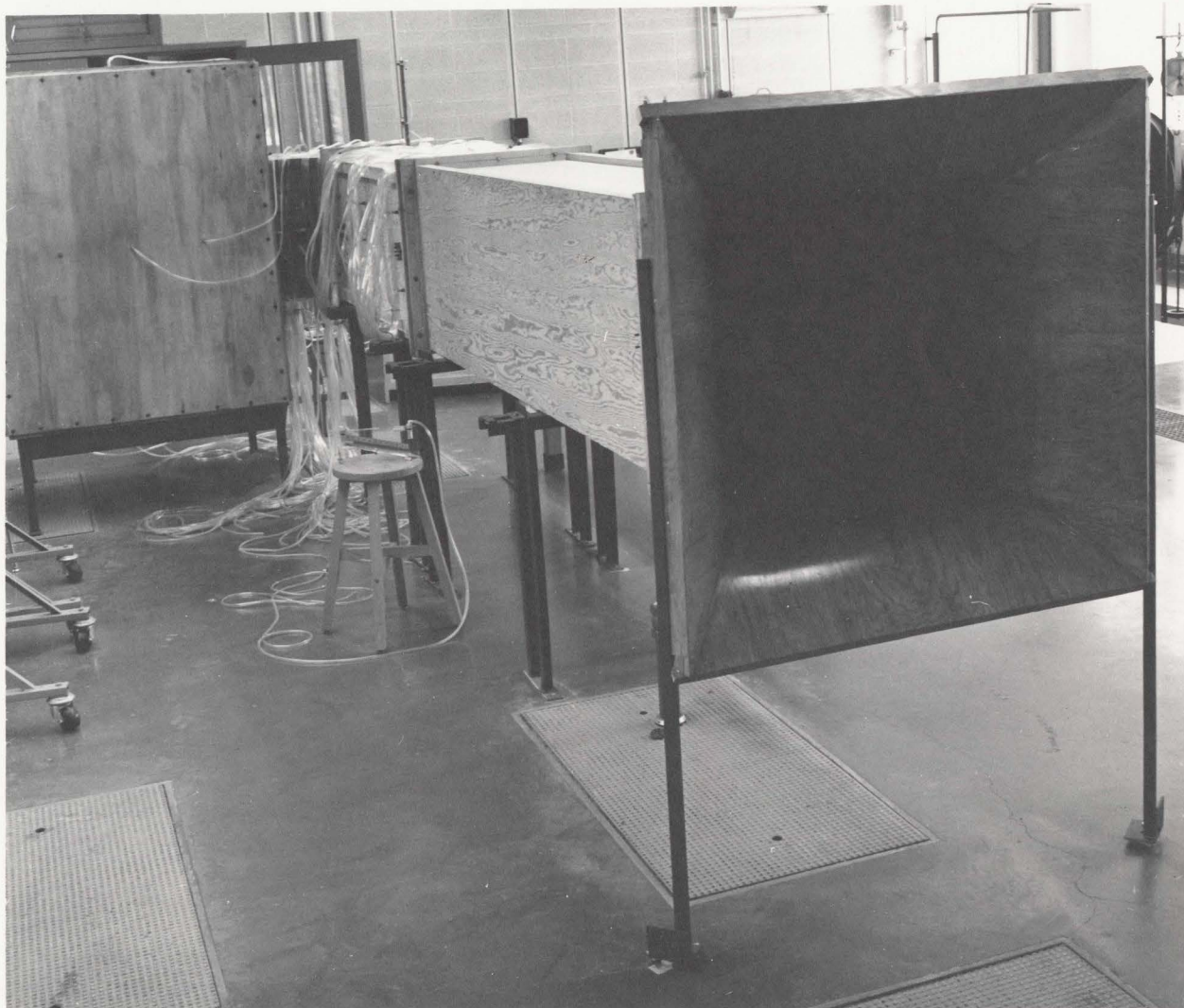
FIGURE 2 (b)

TEST FACILITY - ELBOW DISCHARGING TO PLENUM CHAMBER DIRECTLY
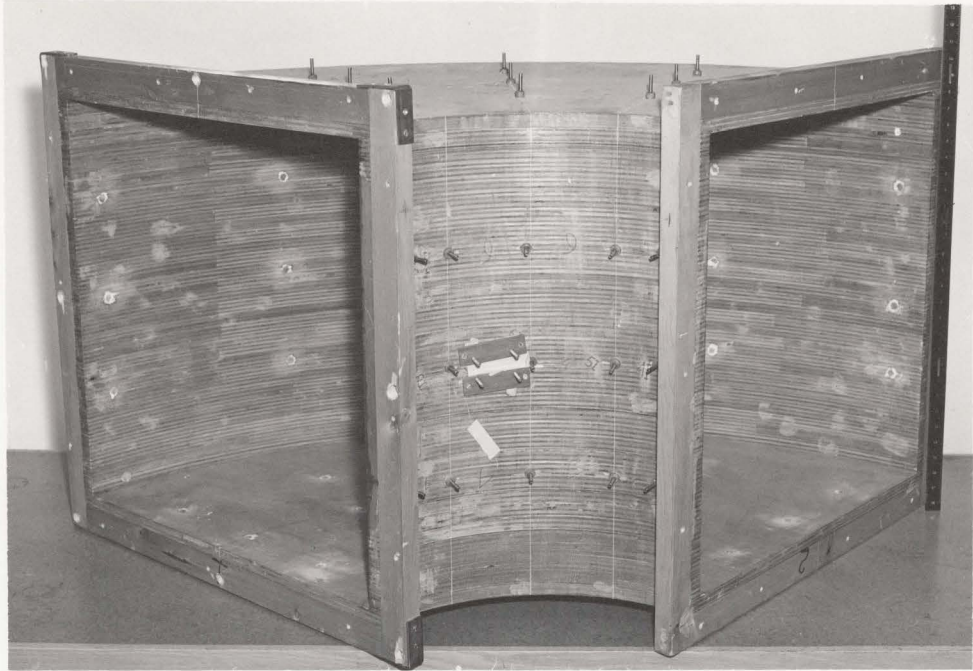
BEND WITH ASPECT RATIO 1

BENDS WITH ASPECT RATIOS 3, 5, & 10

FIGURE 3
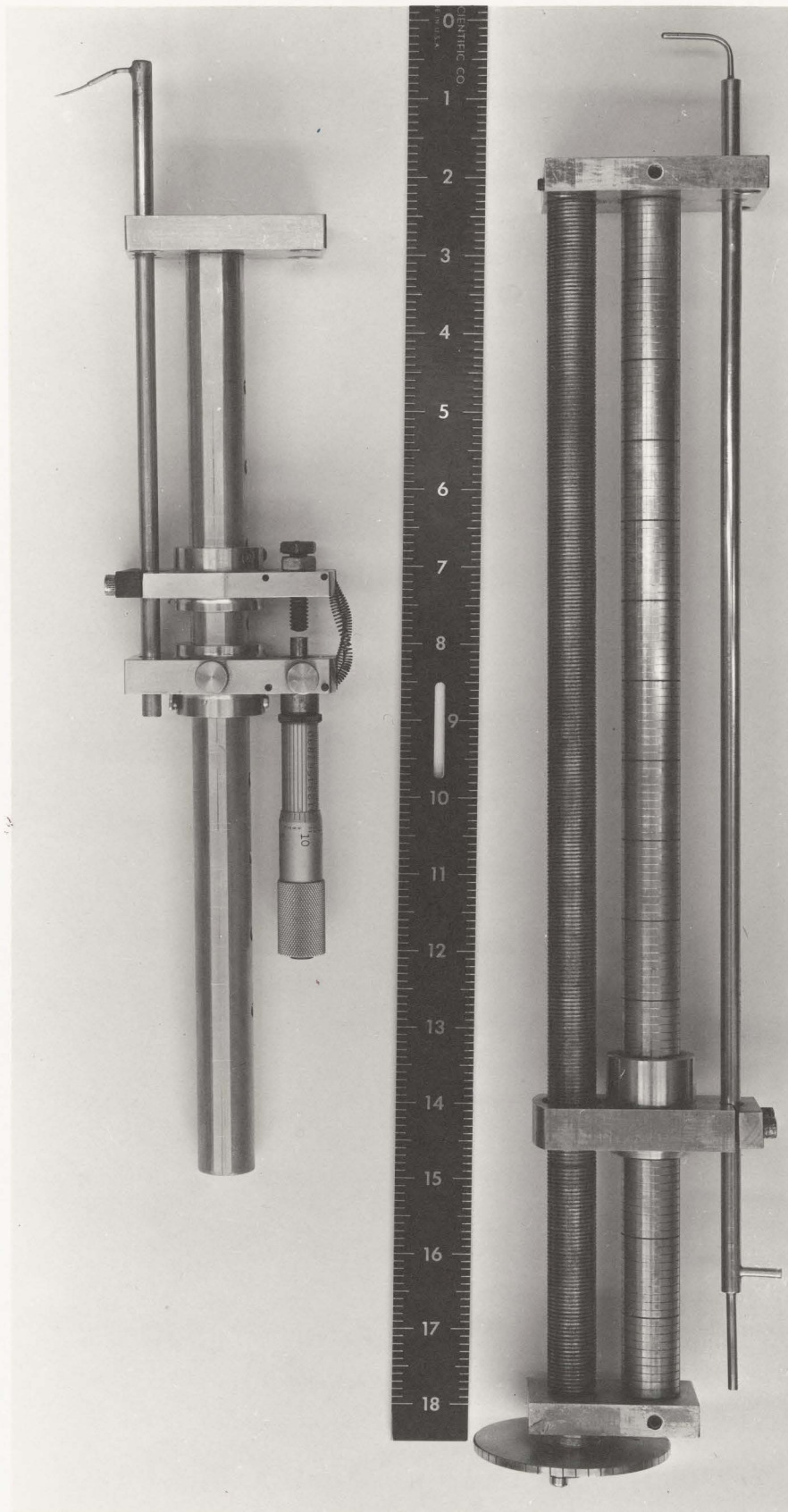
FIGURE 4

TRAVERSING DEVICES
&
VELOCITY PROBES

FIG. NO. 5

o --- SHOWS THE POSITION OF THE LINE OF TRAVERSE WITH RESPECT
TO THE STATIC PRESSURE STATIONS

INSIDE WALL

OUT SIDE WALL
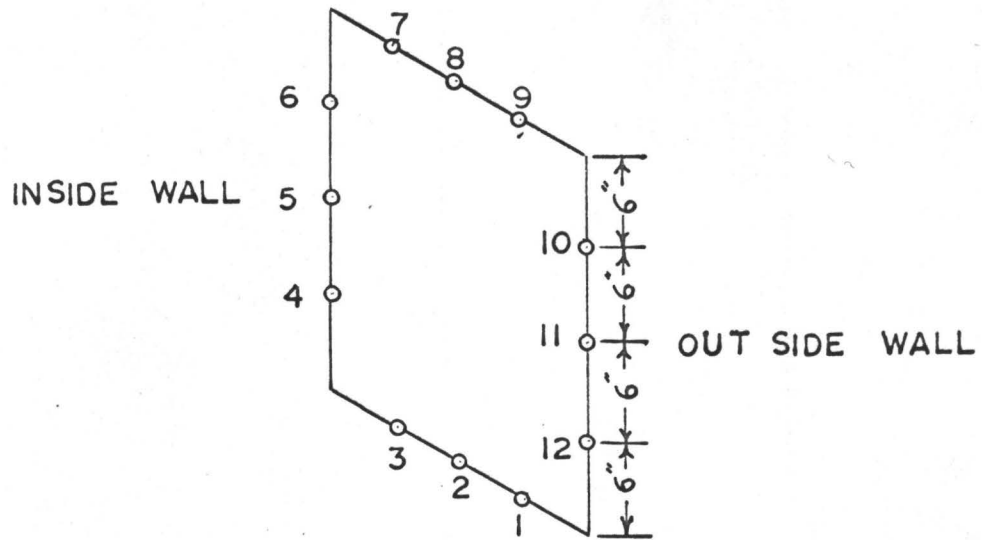
⊙ SHOWS LOCATION OF STATIC PRESSURE
TAP IN 24"x24" DUCT AT ANY STATION

·081"

BRASS

MAHOGANY WOOD

·032" O.D.
HYPODERMIC TUBE (STEEL)
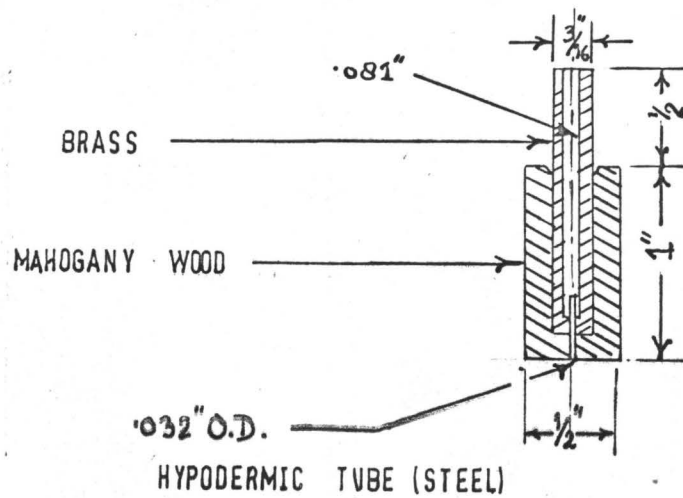
FIG. NO. 6

DETAILS OF THE STATIC PRESSURE TAPS AND THEIR
LOCATION

INSIDE WALL PRESSURE DISTRIBUTION
OBTAINED BY RELAXATION METHOD

OUTSIDE WALL
PRESSURE
DISTRIBUTION
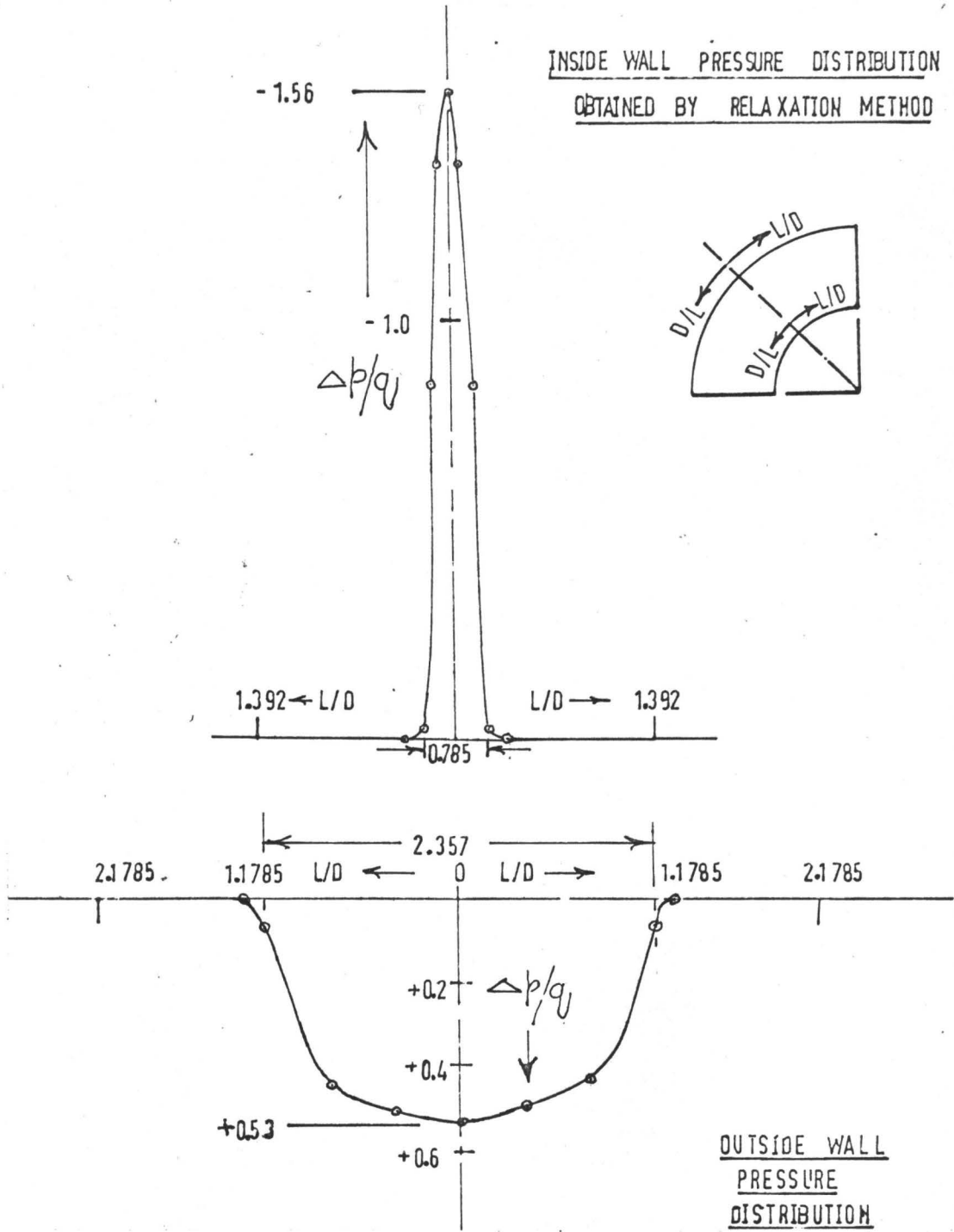
FIG.NO. 7
THEORETICAL PRESSURE DISTRIBUTION
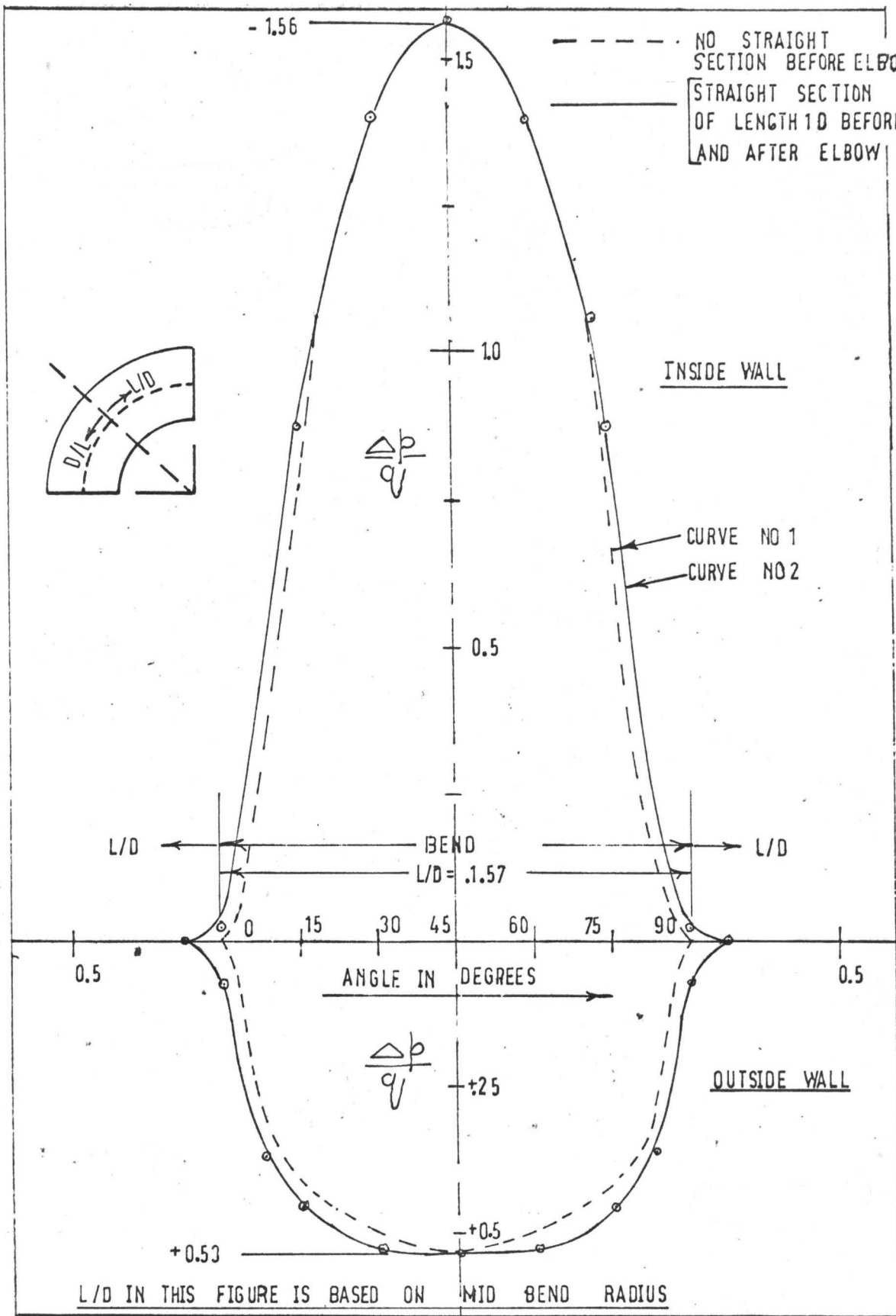
FIGURE NO.8

THEORETICAL PRESSURE DISTRIBUTION

INSIDE WALL PRESSURE
DISTRIBUTION

—— EXPERIMENTAL CURVE
- - - THEORETICAL CURVE TAKEN
FROM FIG NO 7

REYNOLDS NO
⊙ 4.75×10^5
▫ 4.1×10^5
△ 2.9×10^5

BEND
2.357

OUTSIDE WALL PRESSURE
DISTRIBUTION
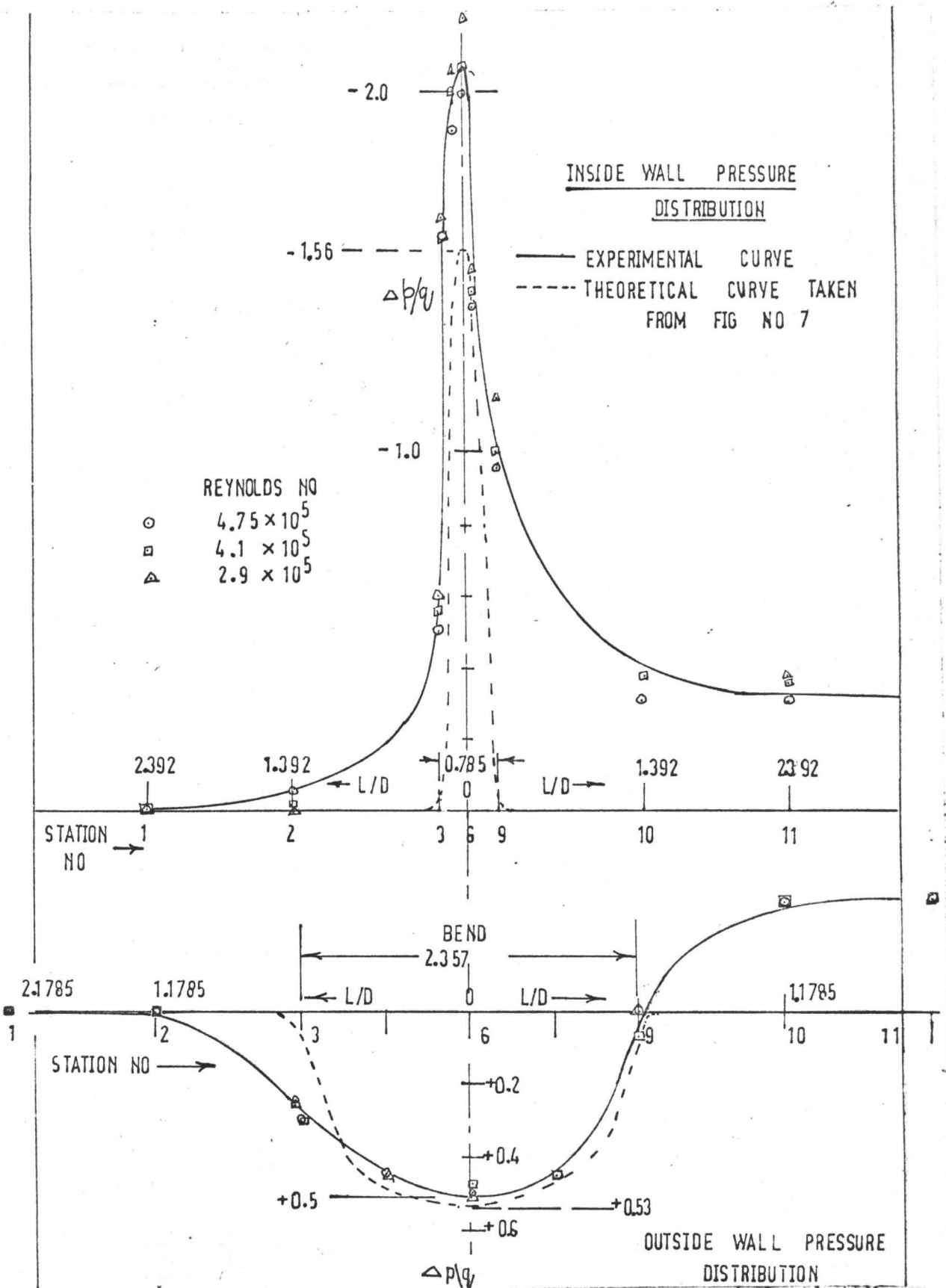
FIG.NO. 9

EXPERIMENTAL PRESSURE DISTRIBUTION

CURVE

CURVE NO 1 ELBOW DISCHARGING TO BOX DIRECTLY

CURVE NO 2 ELBOW DISCHARGING TO BOX THROUGH STRAIGHT DUCT
OF LENGTH 4 D (SAME AS IN FIG NO 9)

EXPERIMENTAL POINTS SHOWN
FOR CURVE NO 1 ONLY

REYNOLDS NO.
4.75 × 10^5
4.1 × 10^5
2.9 × 10^5

INSIDE WALL

CURVE NO 1
CURVE NO 2

$\frac{\Delta p}{q}$

-1.0

-0.8

BOX DUMP
PRESSURE

-0.6

-0.4

STATION NO

L/D=1.57

-0.2

1   2   4   5 6   7   9   10   11

0   22.5 45 67.5 90

BEND

$\frac{\Delta p}{q}$

OUTSIDE WALL

+0.6

L/D HERE IS BASED ON MID BEND RADIUS
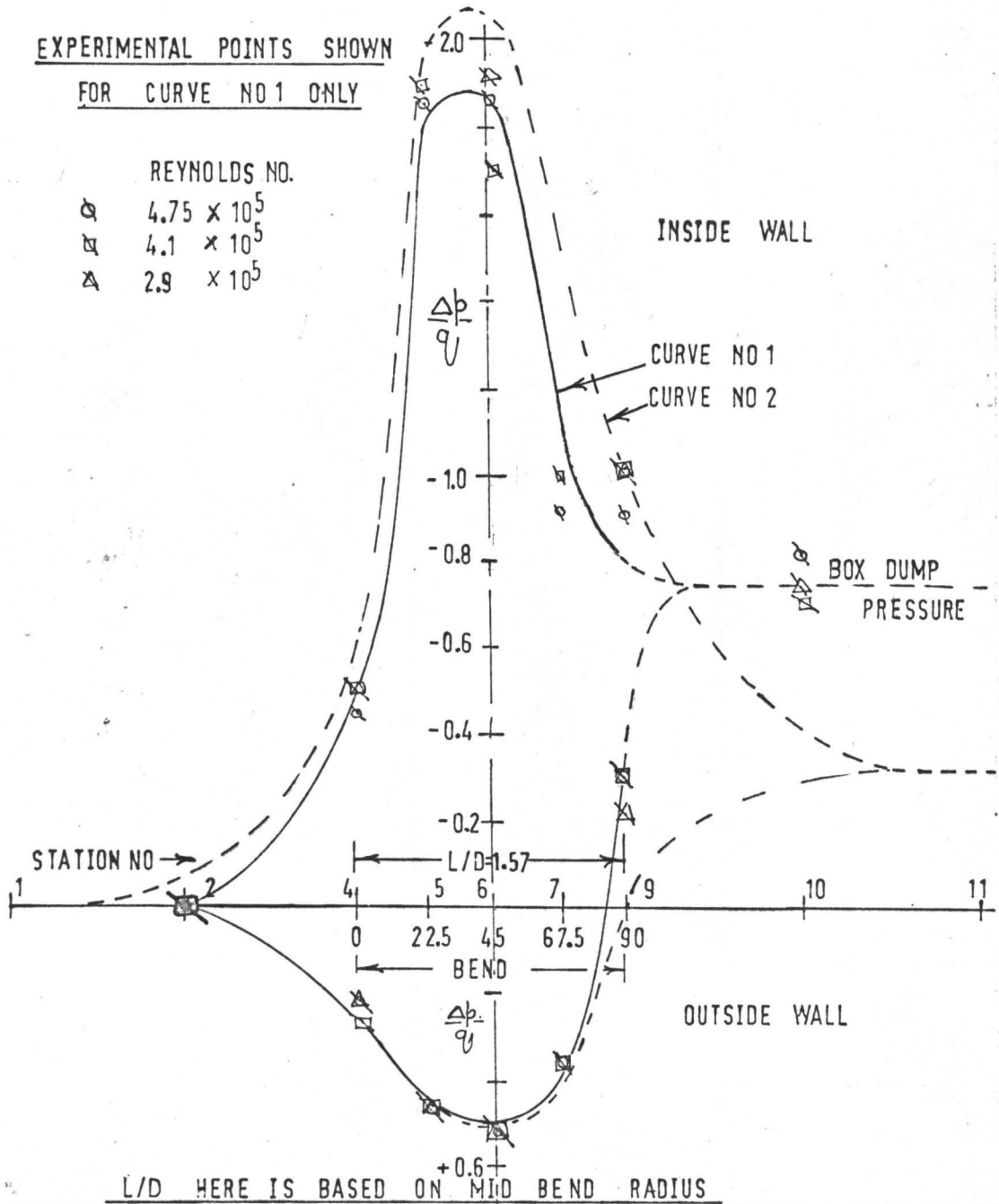
FIG. NO. 10

COMPOSITE PRESSURE DISTRIBUTION CURVE

61
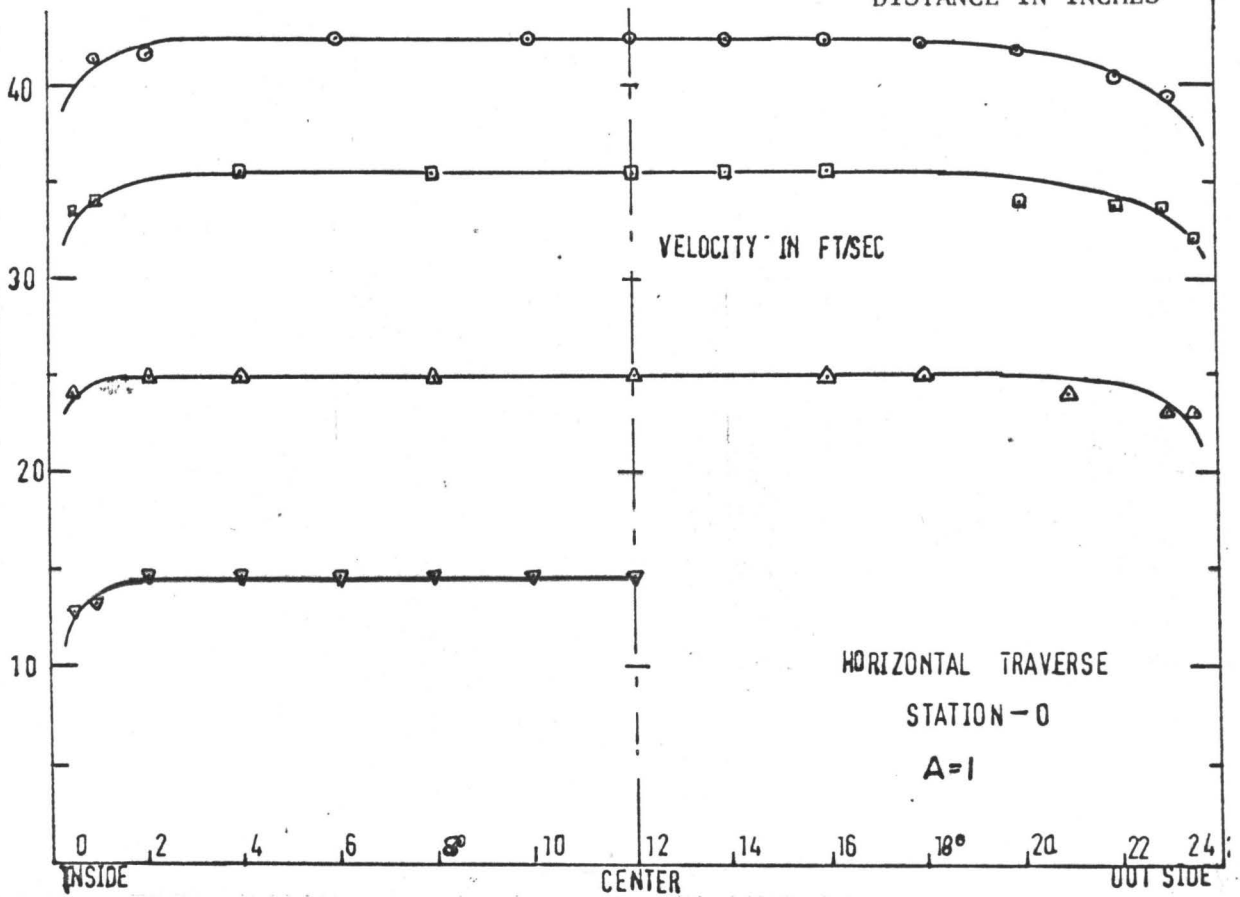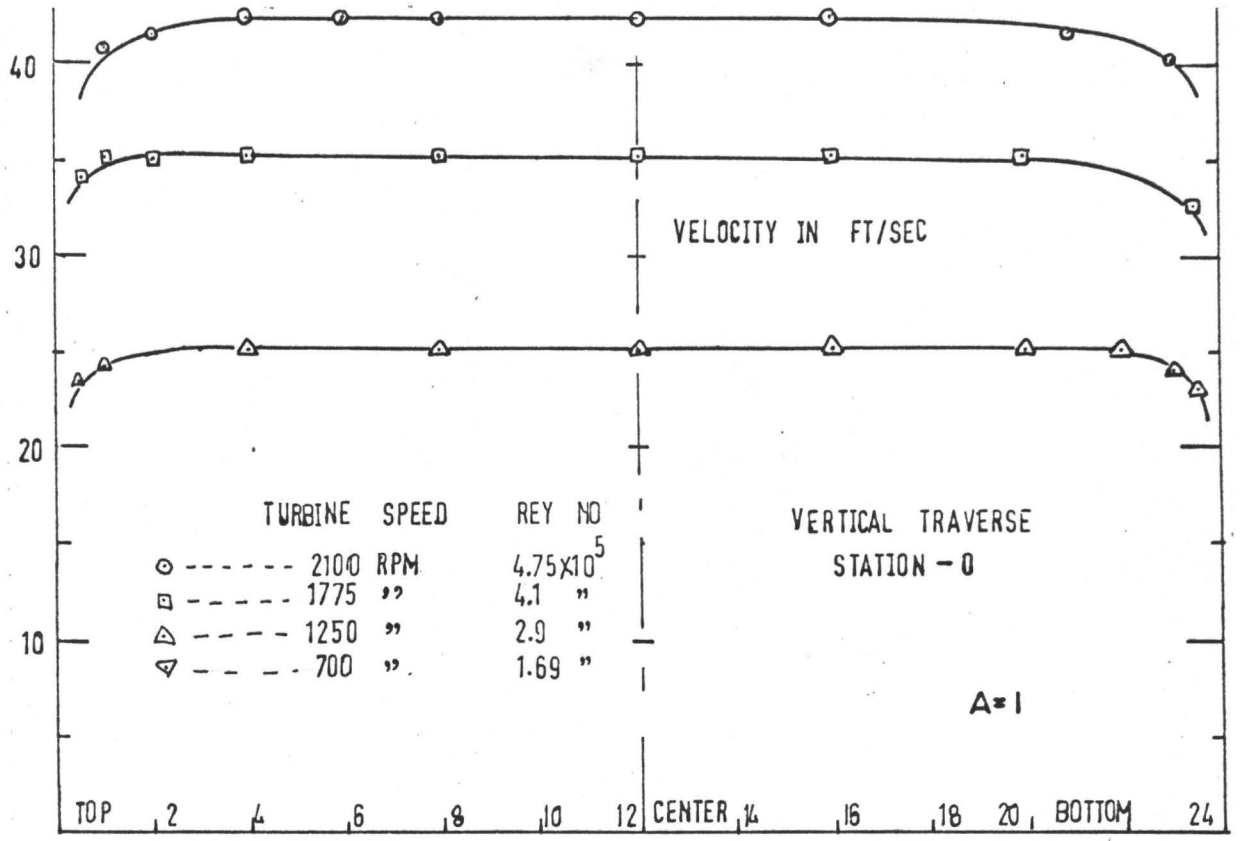
FIG.NO. 11

HORIZONTAL & VERTICAL VELOCITY DISTRIBUTION AT AN A= 1
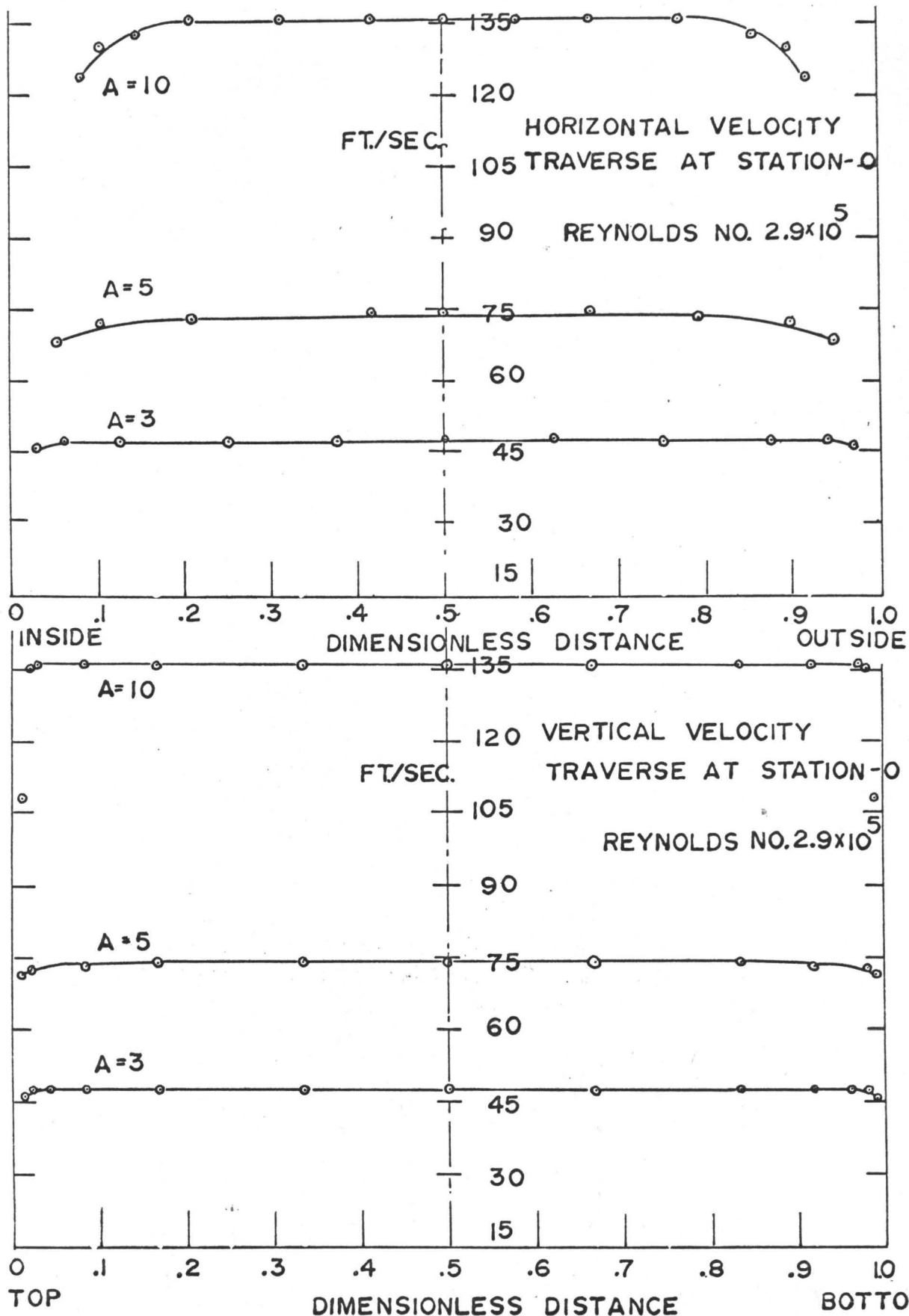
FIG. NO. 12

HORIZONTAL & VERTICAL VELOCITY DISTRIBUTION AT A= 3,5 & 10

VELOCITY IN FT/SEC AT STATION 6

REY. NO. 4.1×10^5

TURBINE SPEED 1250
"   "   1775

REY. NO. 2.9 ×10^5

FIG.NO.13
HORIZONTAL VELOCITY TRAVERSE
AT STATION 6

OUTSIDE
24   20   16   12   8   4   INSIDE
0

STATION NO.
▽   1
⊟   3
⊙   6
⊘   13
⌀   9

TURBINE SPEED 2100
REY. NO. 4.75×10^5

VELOCITY IN FT/SEC

FIG.NO. 14
HORIZONTAL VELOCITY TRAVERSE
AT DIFFERENT STATIONS

24   20   16   12   8   4   0
OUTSIDE   DISTANCE IN INCHES   INSIDE
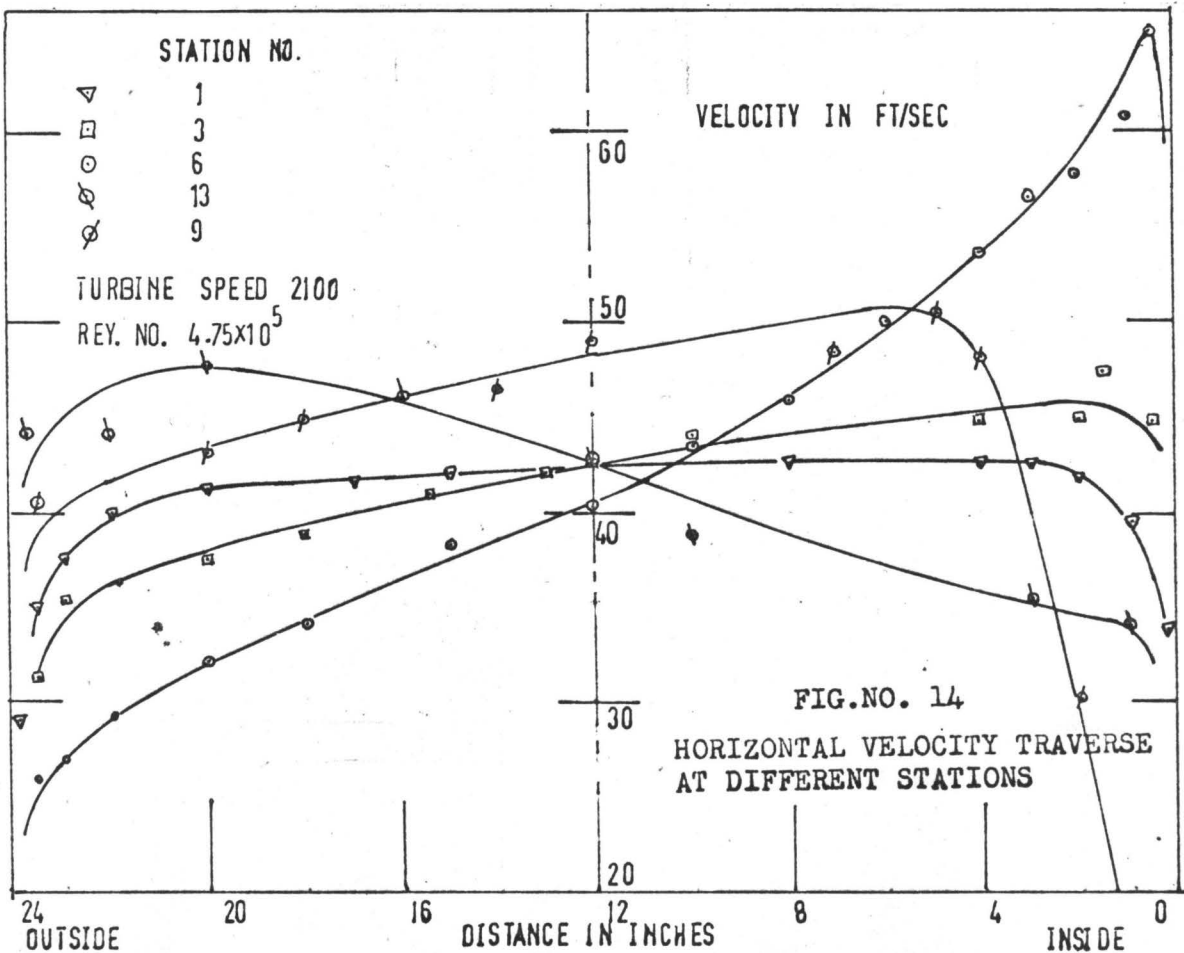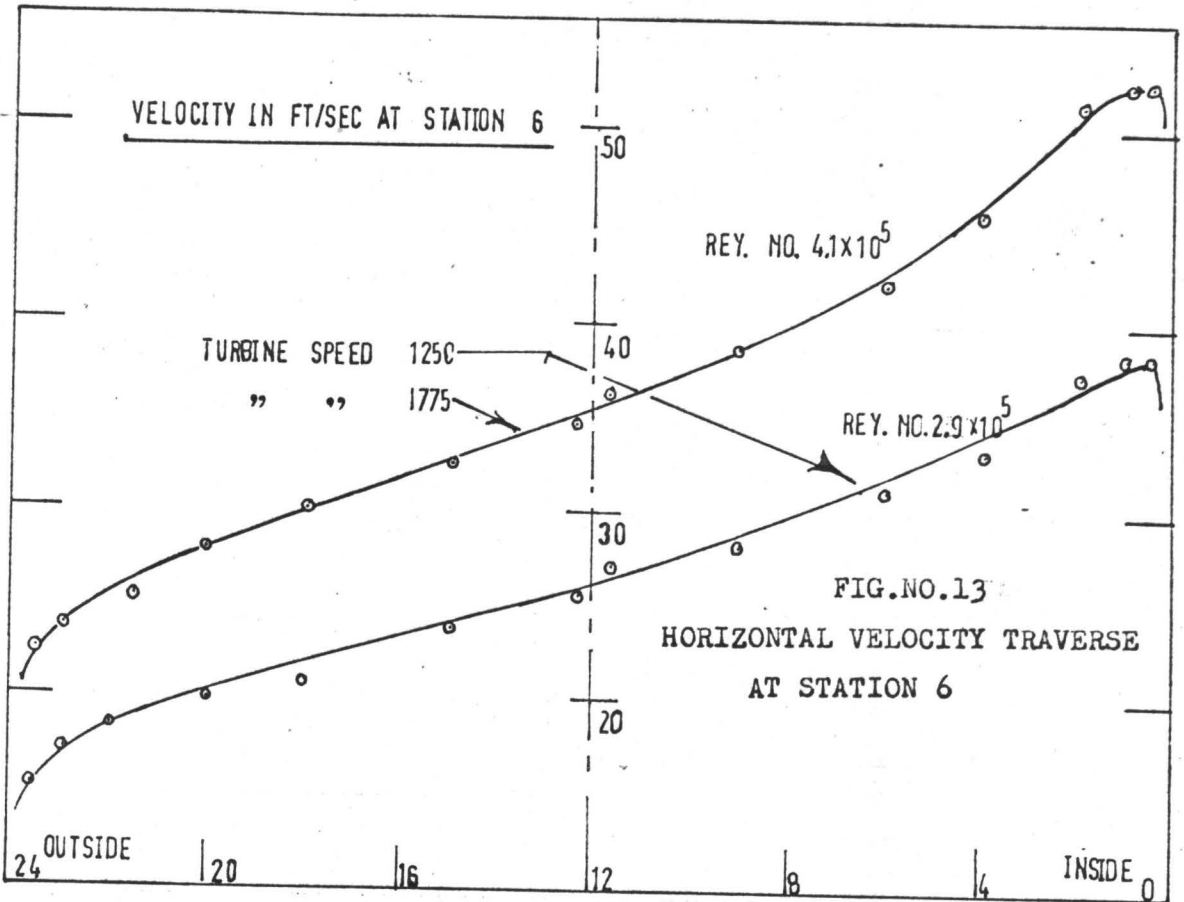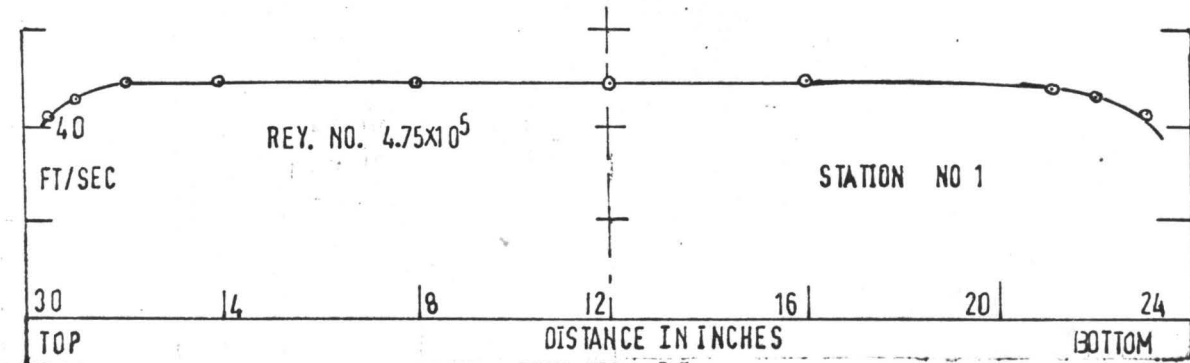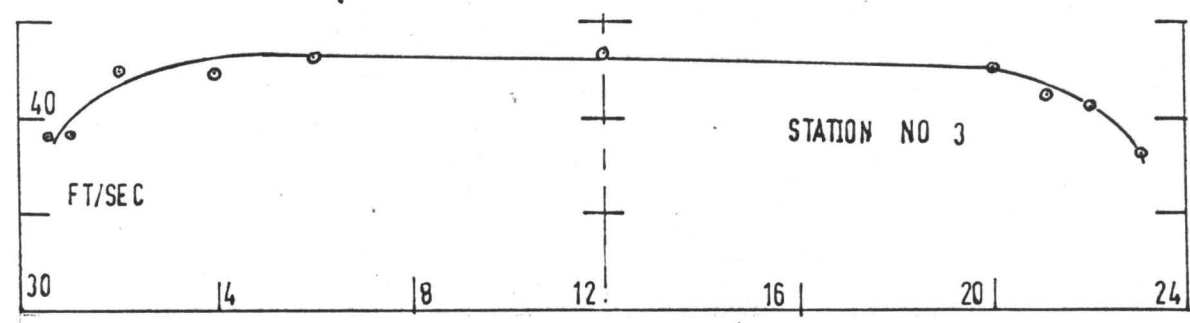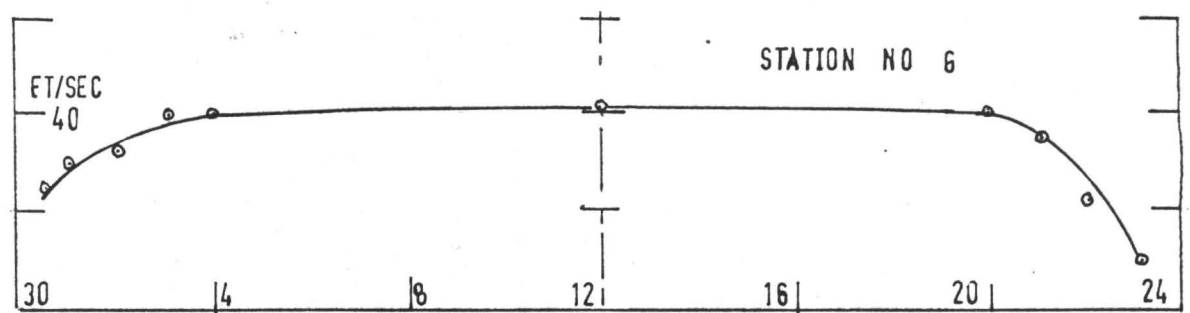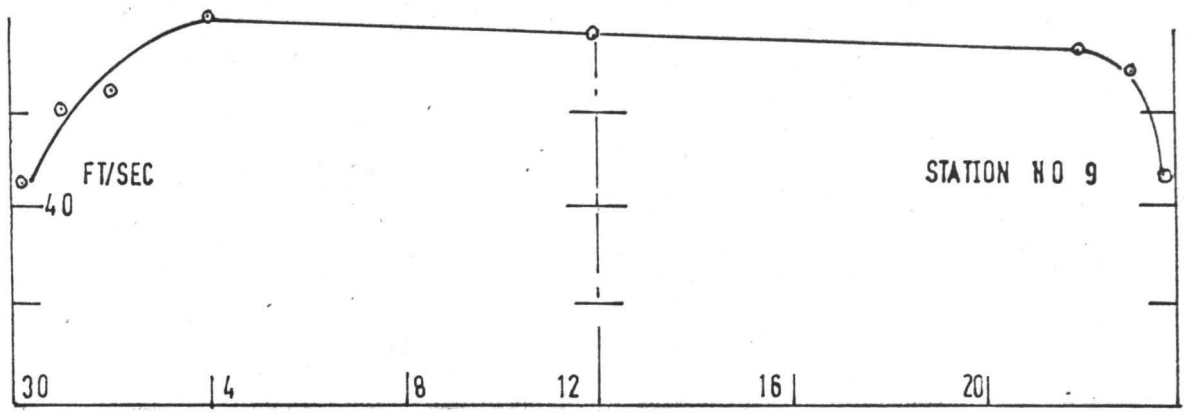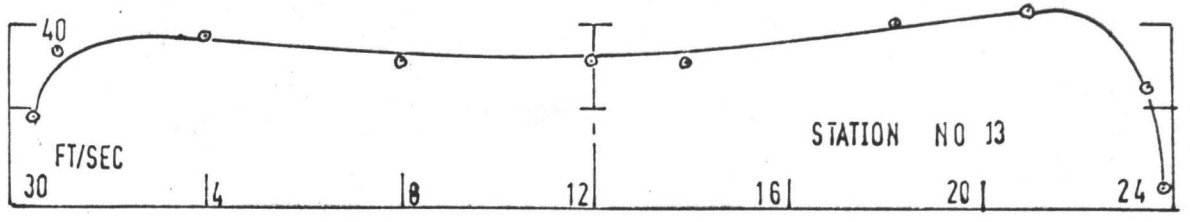
FIG.NO. 15

VERTICAL VELOCITY TRAVERSES TAKEN AT A NUMBER OF STATIONS
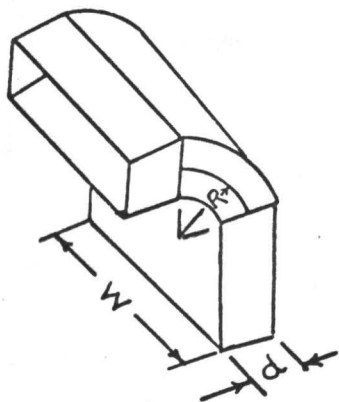
FIG.NO.16
NOMENCLATURE FOR BEND
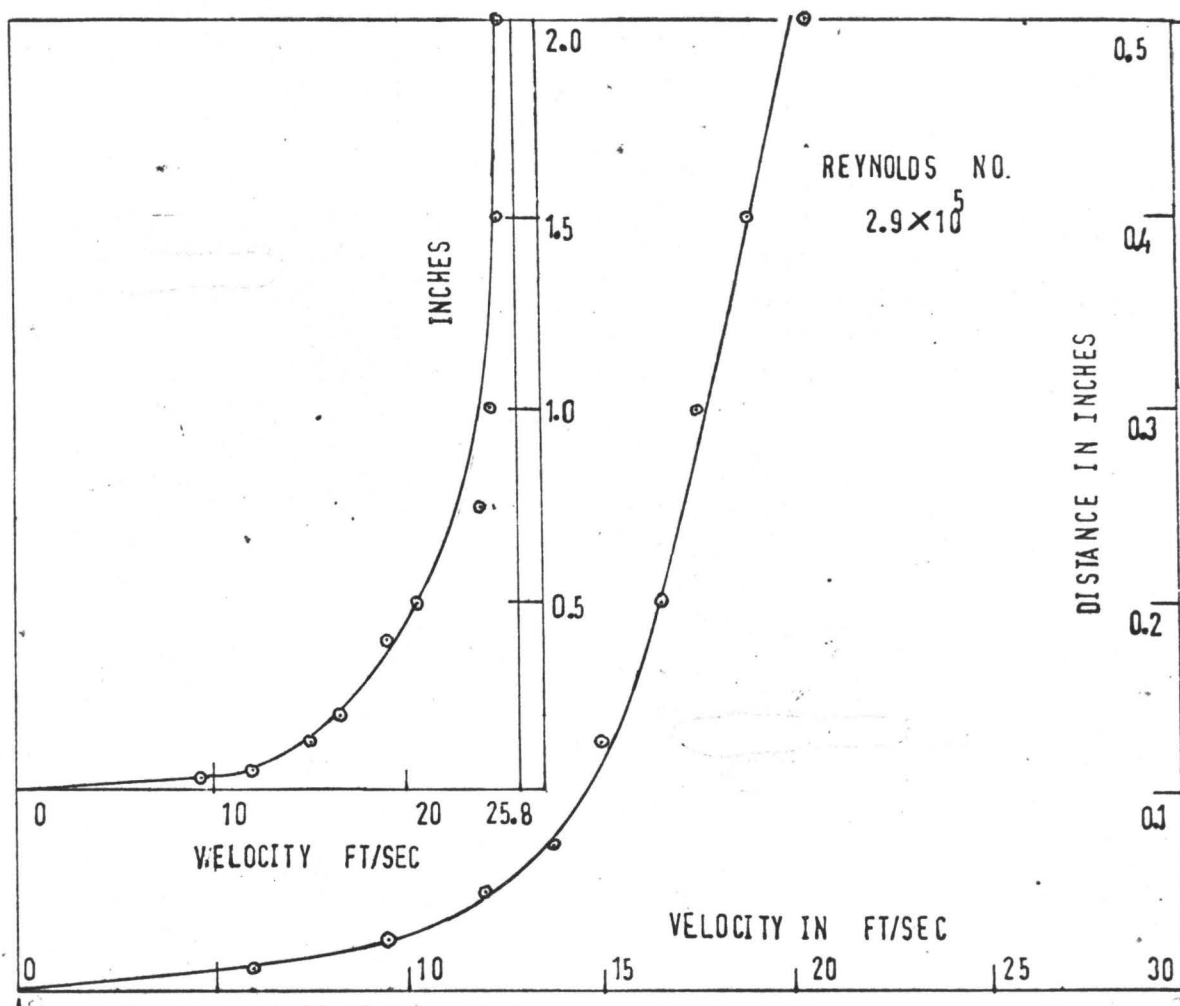
FIG.NO. 17

BOUNDARY LAYER PROFILE ON INSIDE WALL AT STATION NO.1

Re = 2.9 x 10^5

FIG.NO.18
BOUNDARY LAYER
PROFILE ON INSIDE
WALL AT STATION 1
Re= 4.75x10⁵

FIG.NO.19
BOUNDARY LAYER PROFILE
ON INSIDE WALL AT
STATION 1

Re = 4.1 x 10⁵
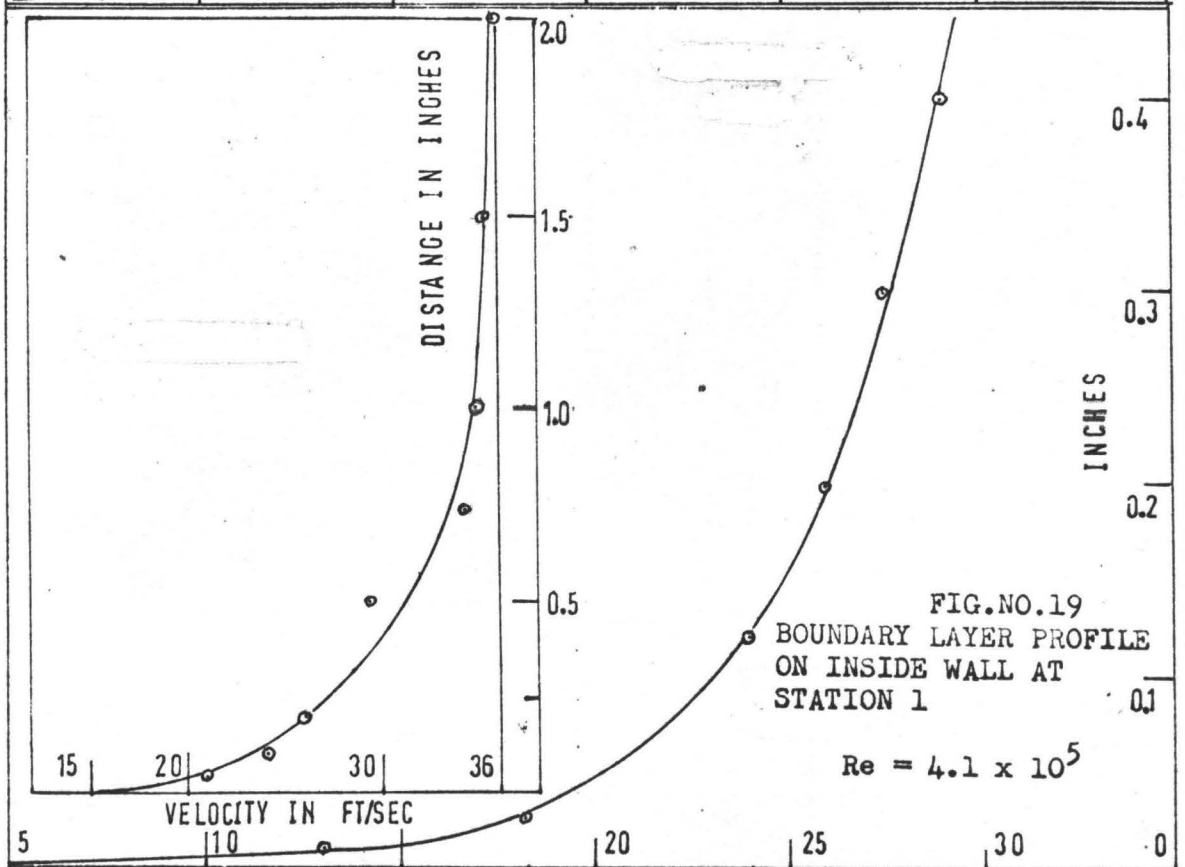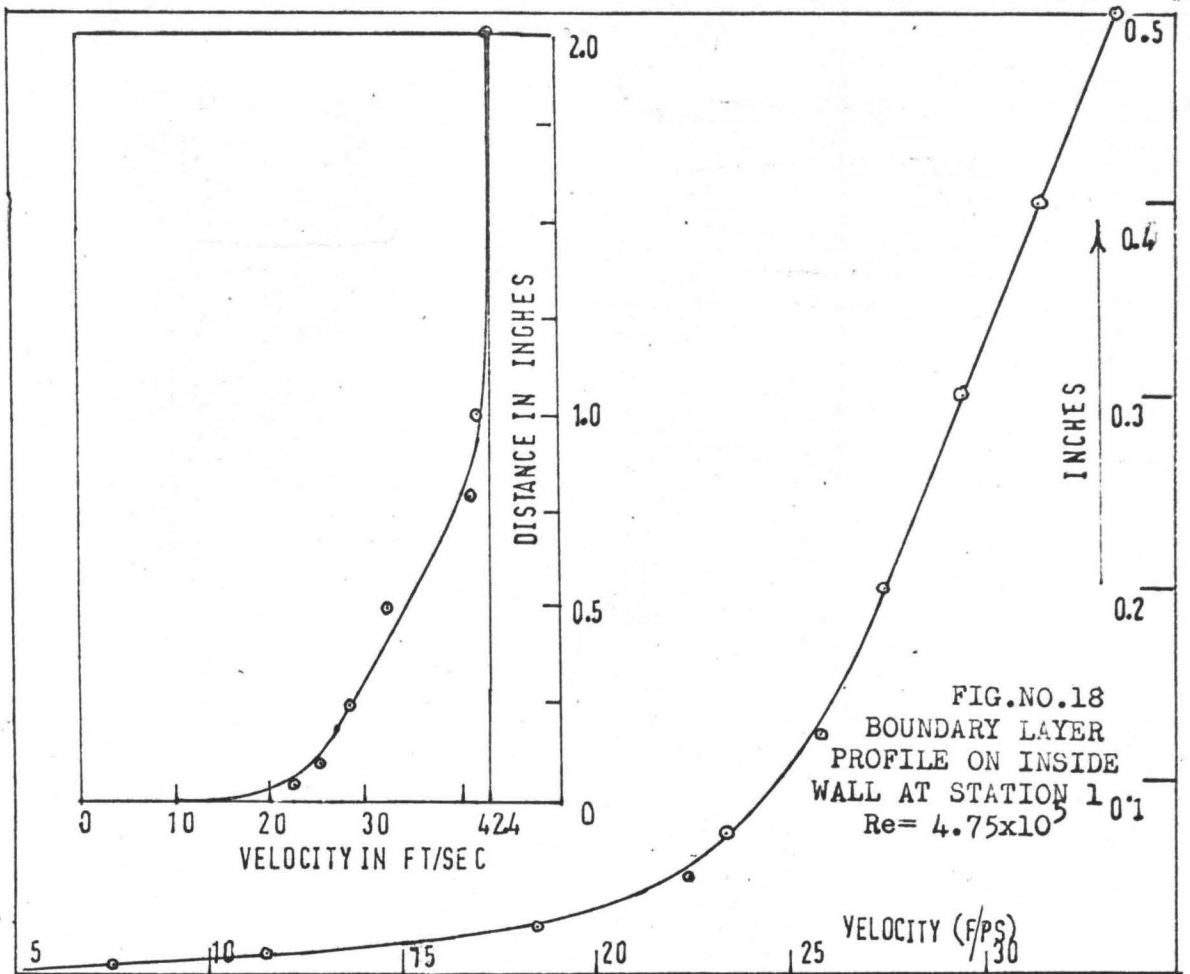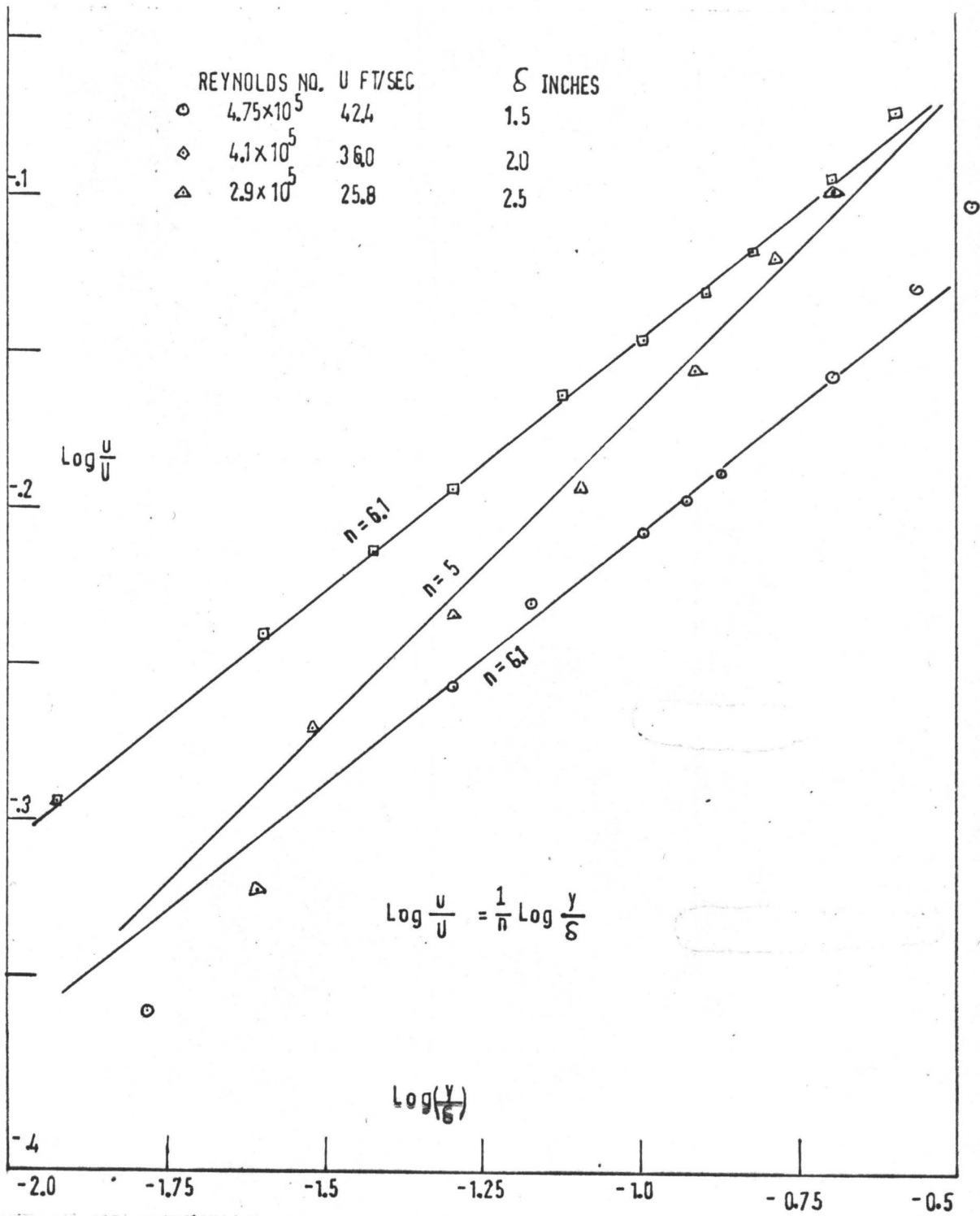
FIG. NO. 20

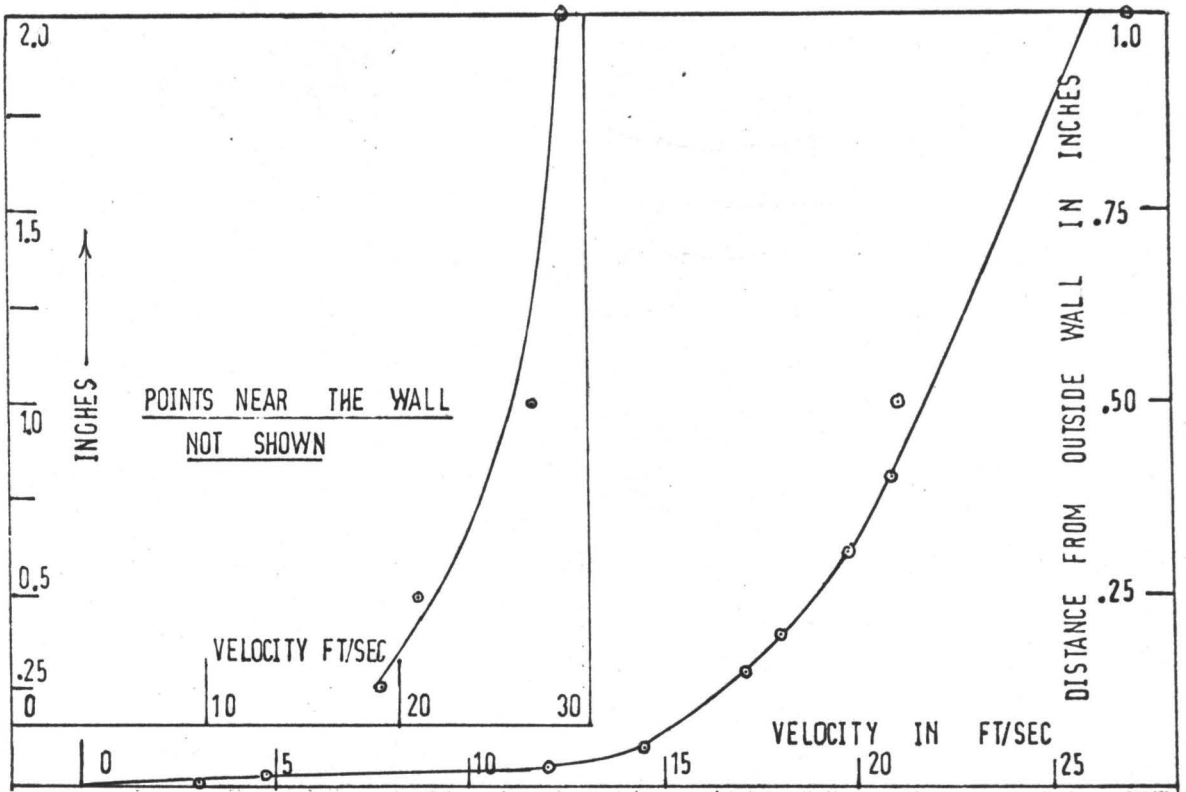BOUNDARY LAYER VELOCITY PROFILE (LOG PLOT) AT STATION NO. 1

ON INSIDE WALL
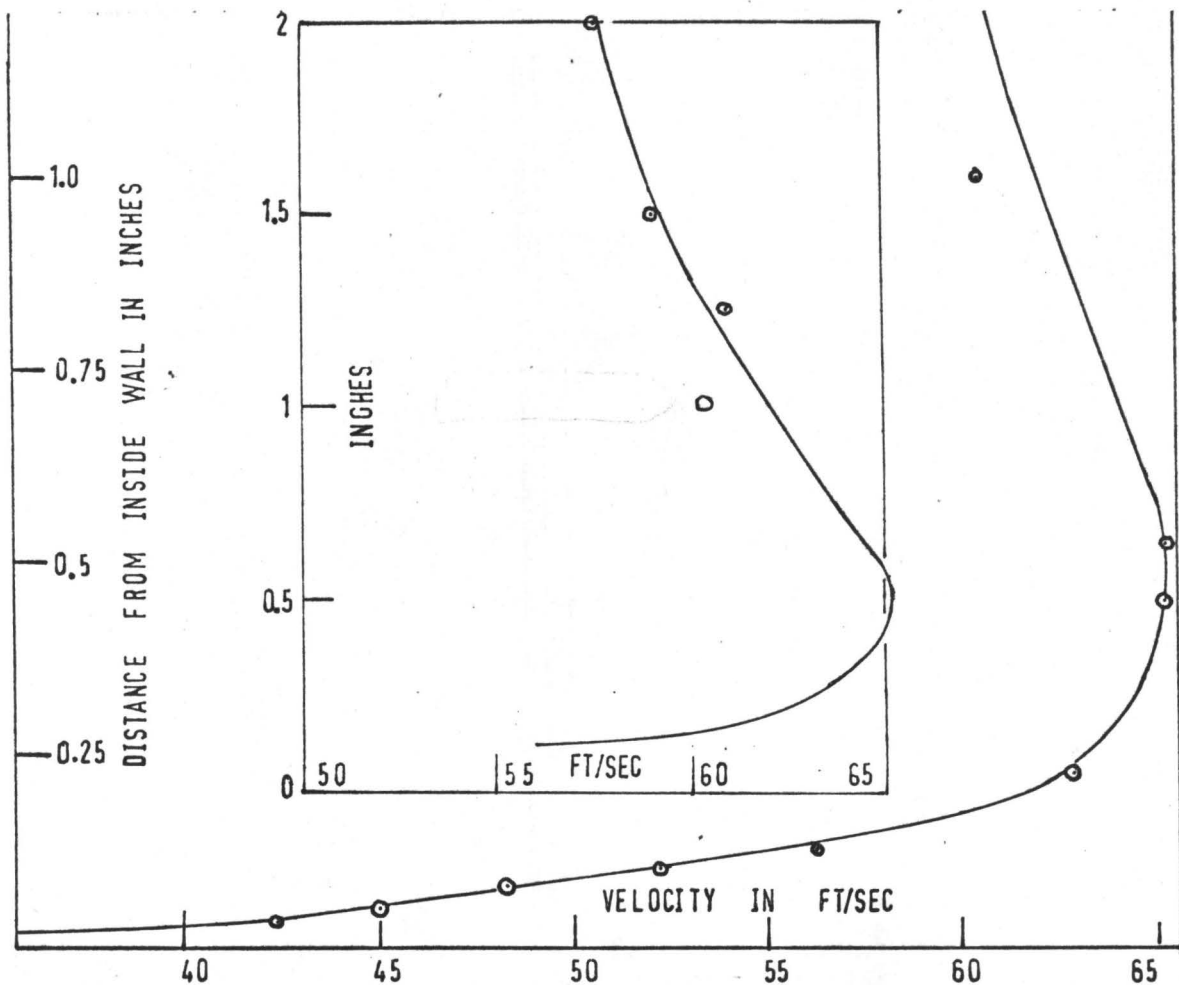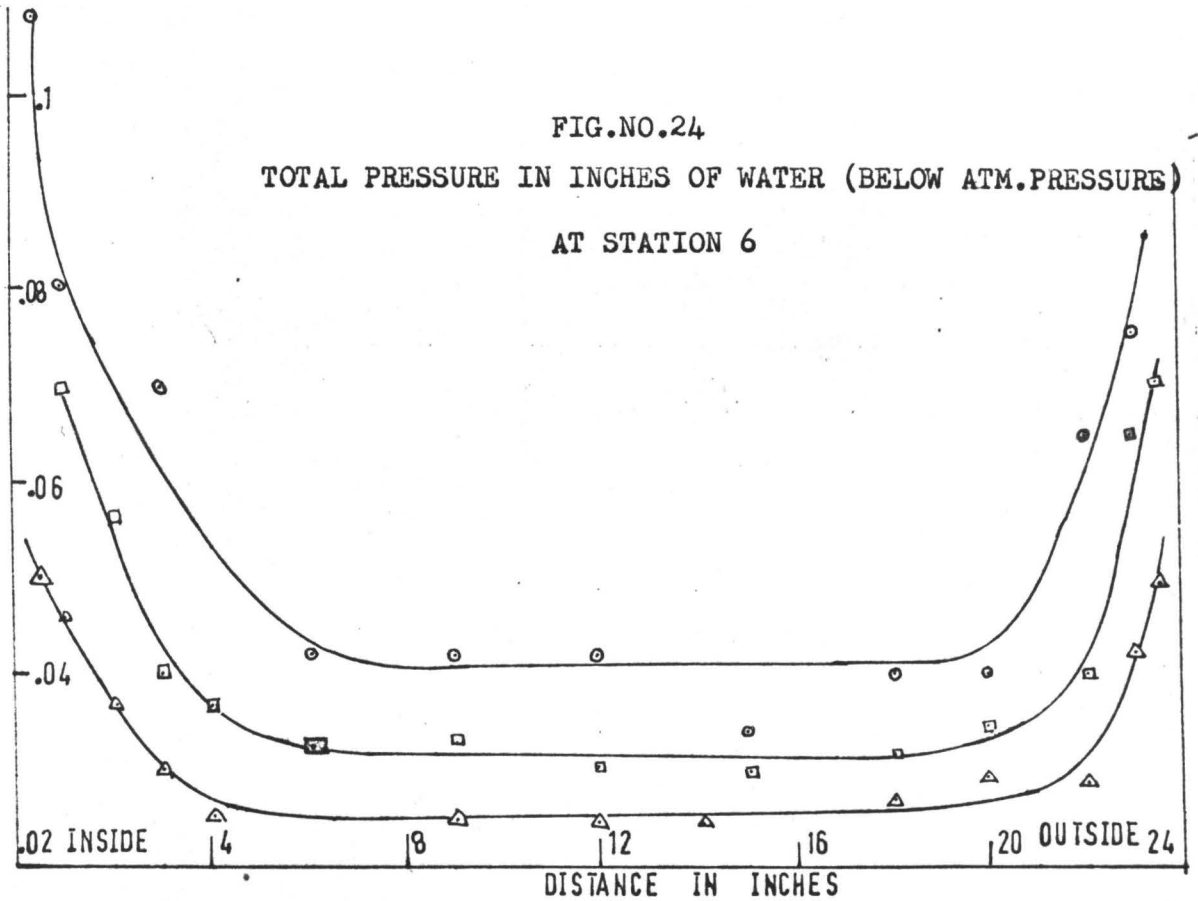
FIG.NO.21

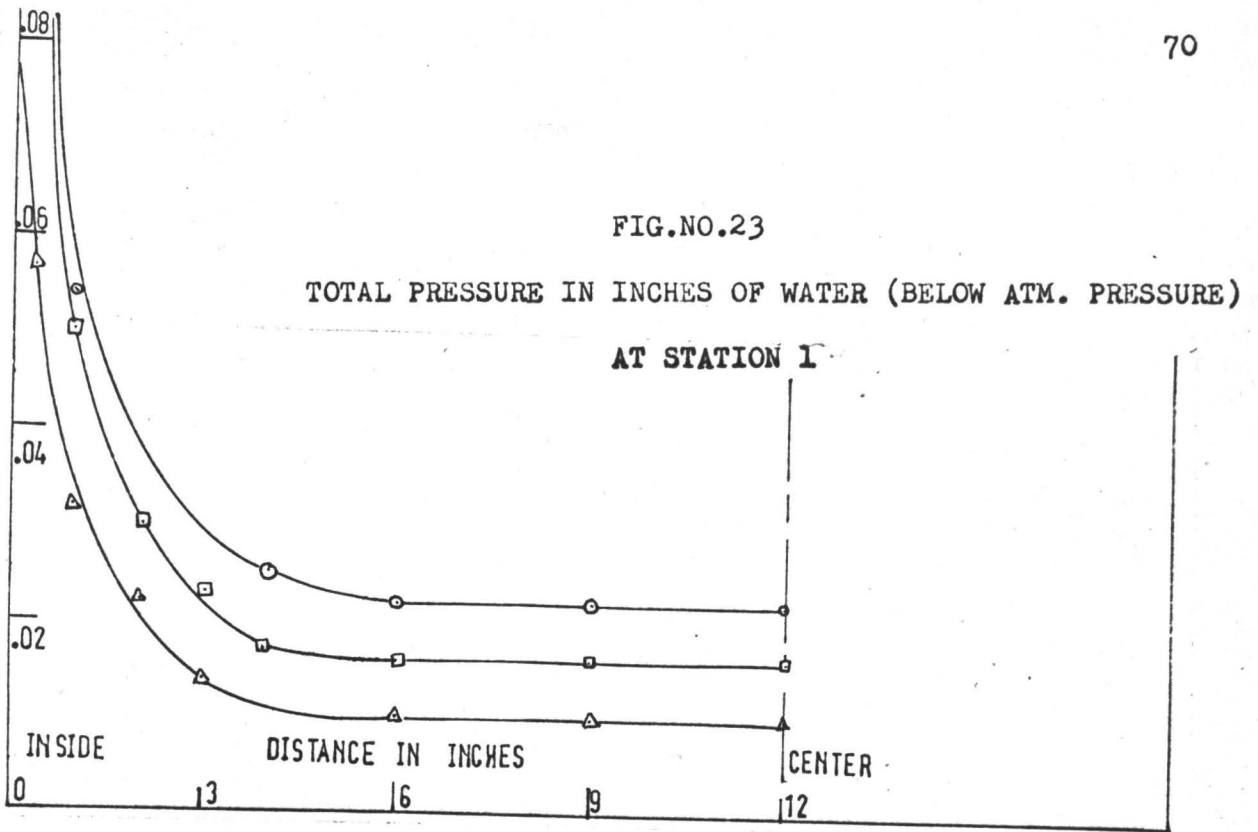VELOCITY PROFILE AT STATION 6 ON THE OUTSIDE WALL Re=4.75 x 10^5

FIG. NO. 22

VELOCITY PROFILE AT STATION 6 ON THE INSIDE WALL   Re=4.75 x 10^5

FIG.NO.23

TOTAL PRESSURE IN INCHES OF WATER (BELOW ATM. PRESSURE)

AT STATION 1

FIG.NO.24

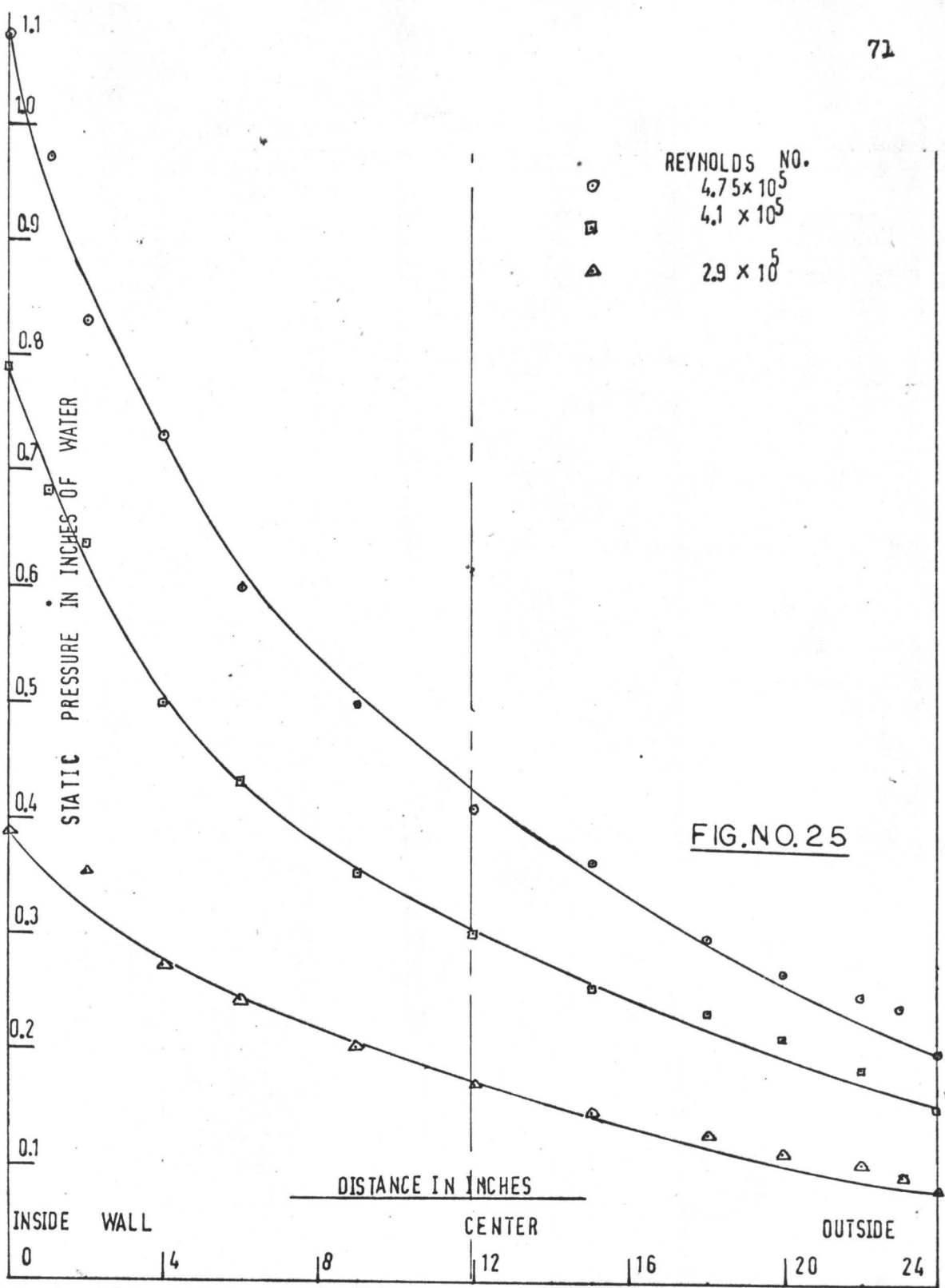TOTAL PRESSURE IN INCHES OF WATER (BELOW ATM.PRESSURE)

AT STATION 6

FIG.NO.25

THE CALCULATED STATIC PRESSURES IN INCHES OF WATER(BELOW
ATM.PRESSURE) AT STATION 6

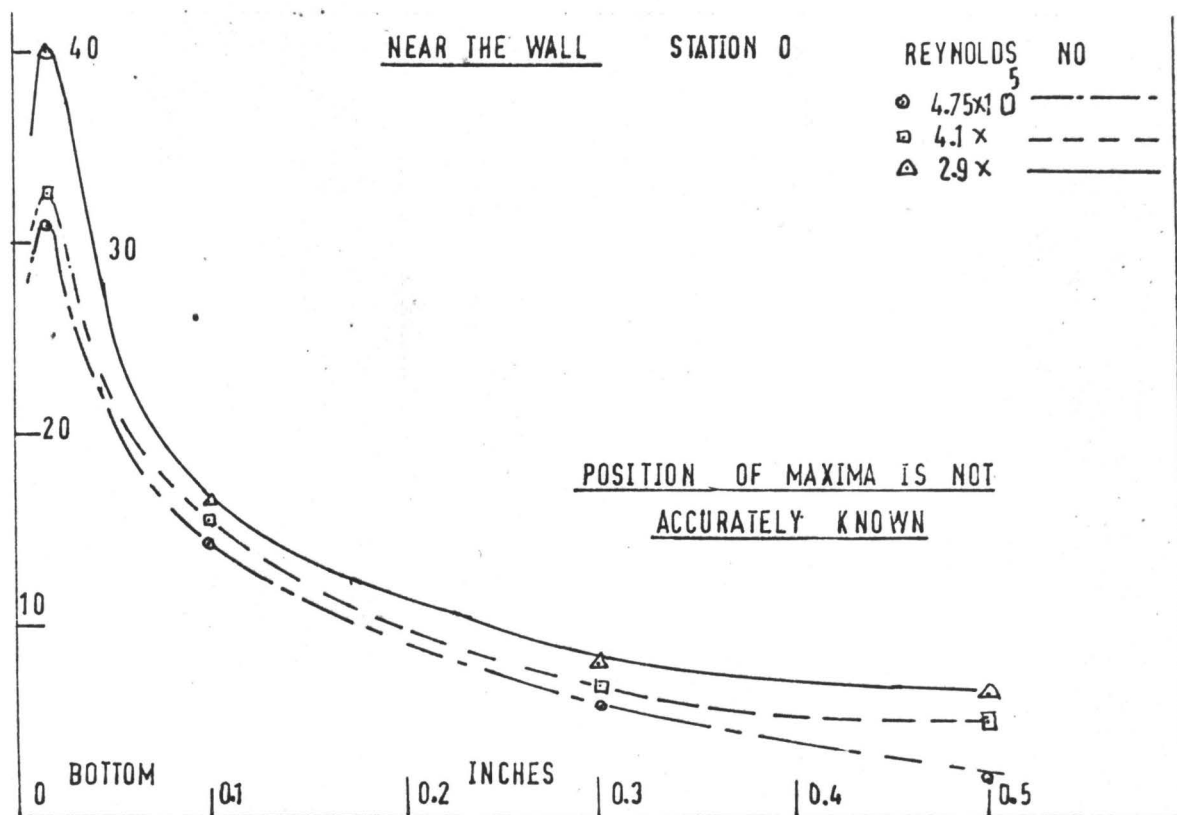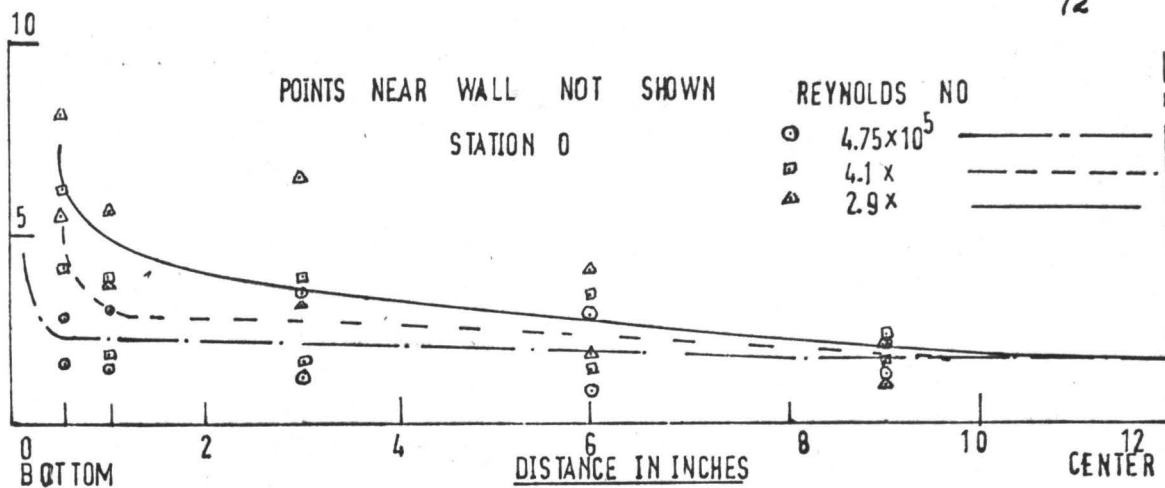FIG.NO.26

PERCENTAGE VALUES OF THE TURBULENCE LEVEL IN THE
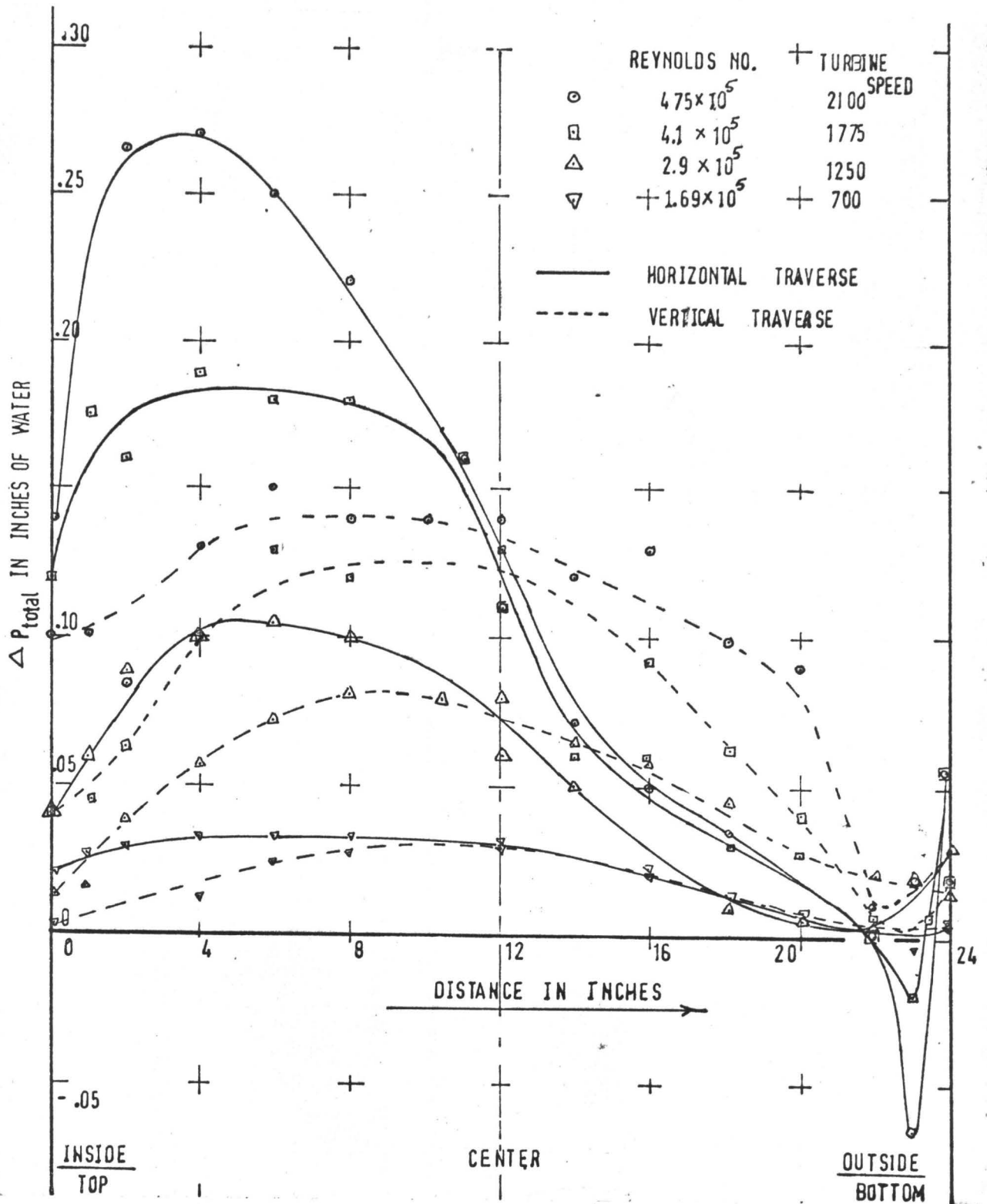
FREE STREAM AND NEAR THE WALL
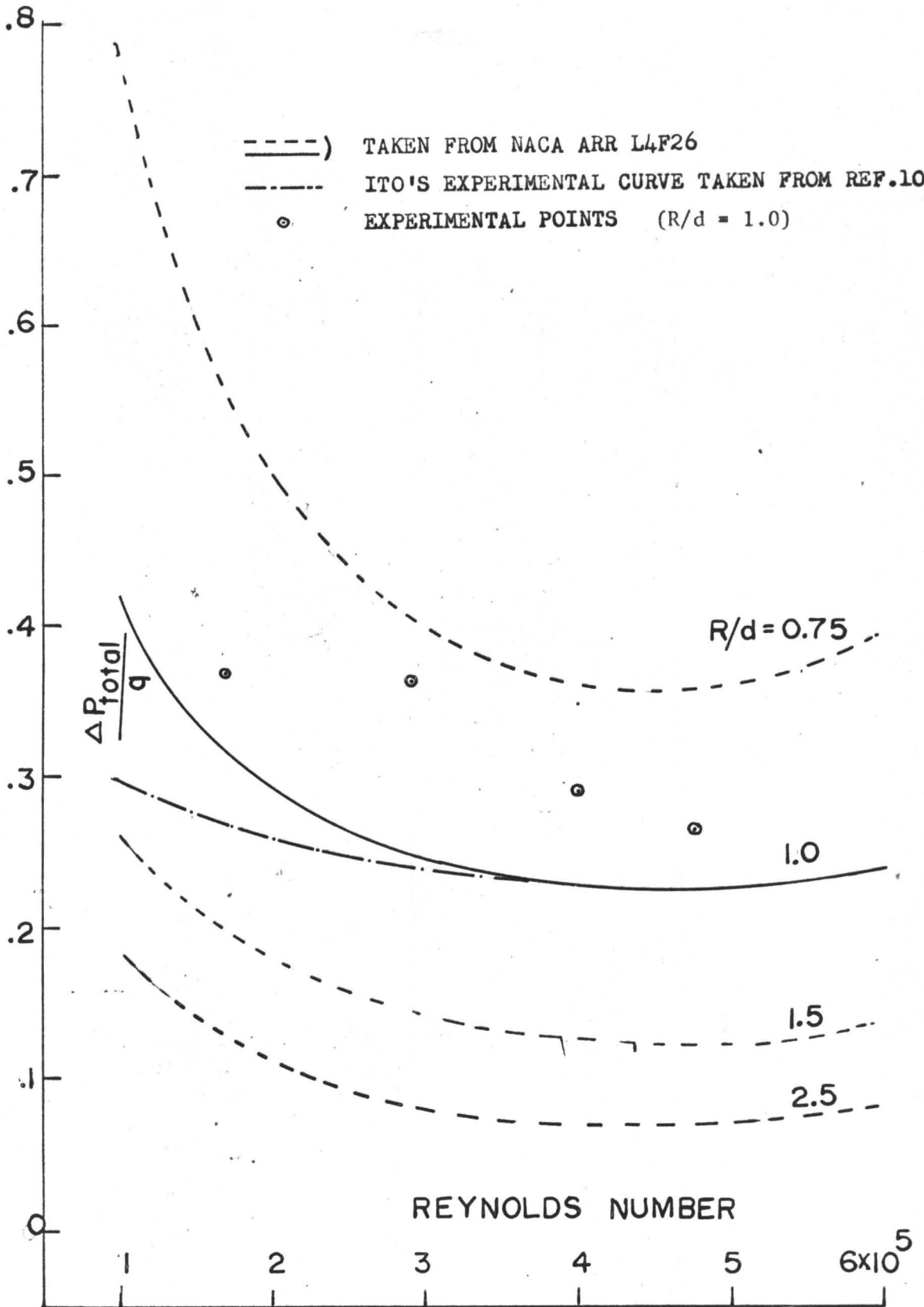
FIG.NO. 27

LOSS IN TOTAL PRESSURE IN INCHES OF WATER

FIG.NO.28(a)

TOTAL PRESSURE LOSS ACROSS ELBOW WHEN IT IS DISCHARGING

TO PLENUM CHAMBER THROUGH 4D LONG DUCT

FOR A = 1.0

- - - -) TAKEN FROM NACA ARR L4F26
⊙   EXPERIMENTAL POINTS (R/d = 1.0)

R/d= 0.75

$\dfrac{\triangle P_{total}}{q}$

1.0

1.5

2.5

REYNOLDS NUMBER
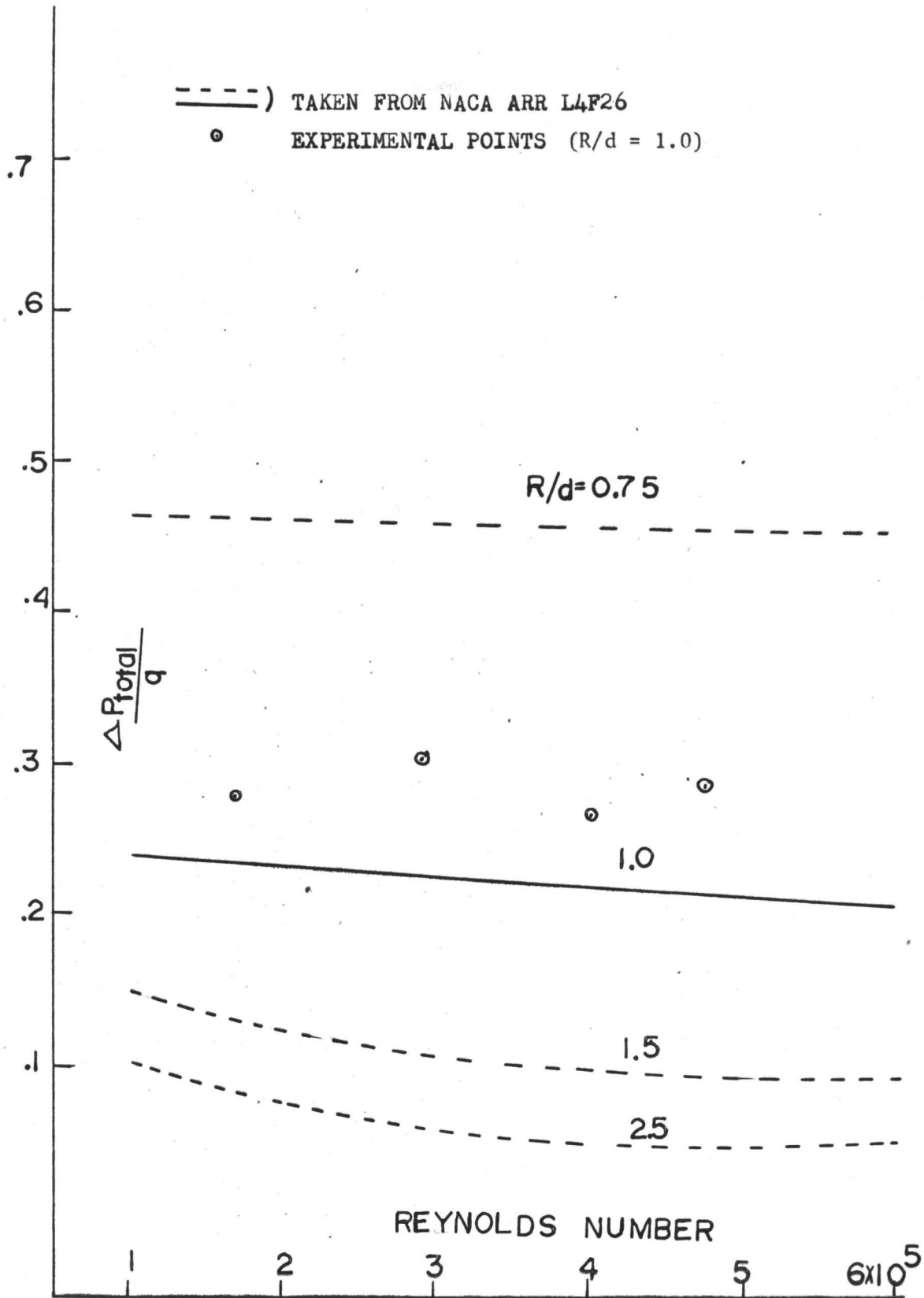
1   2   3   4   5   6x10^5

FIG.NO.28(b)

TOTAL PRESSURE LOSS ACROSS ELBOW WHEN IT IS DISCHARGING
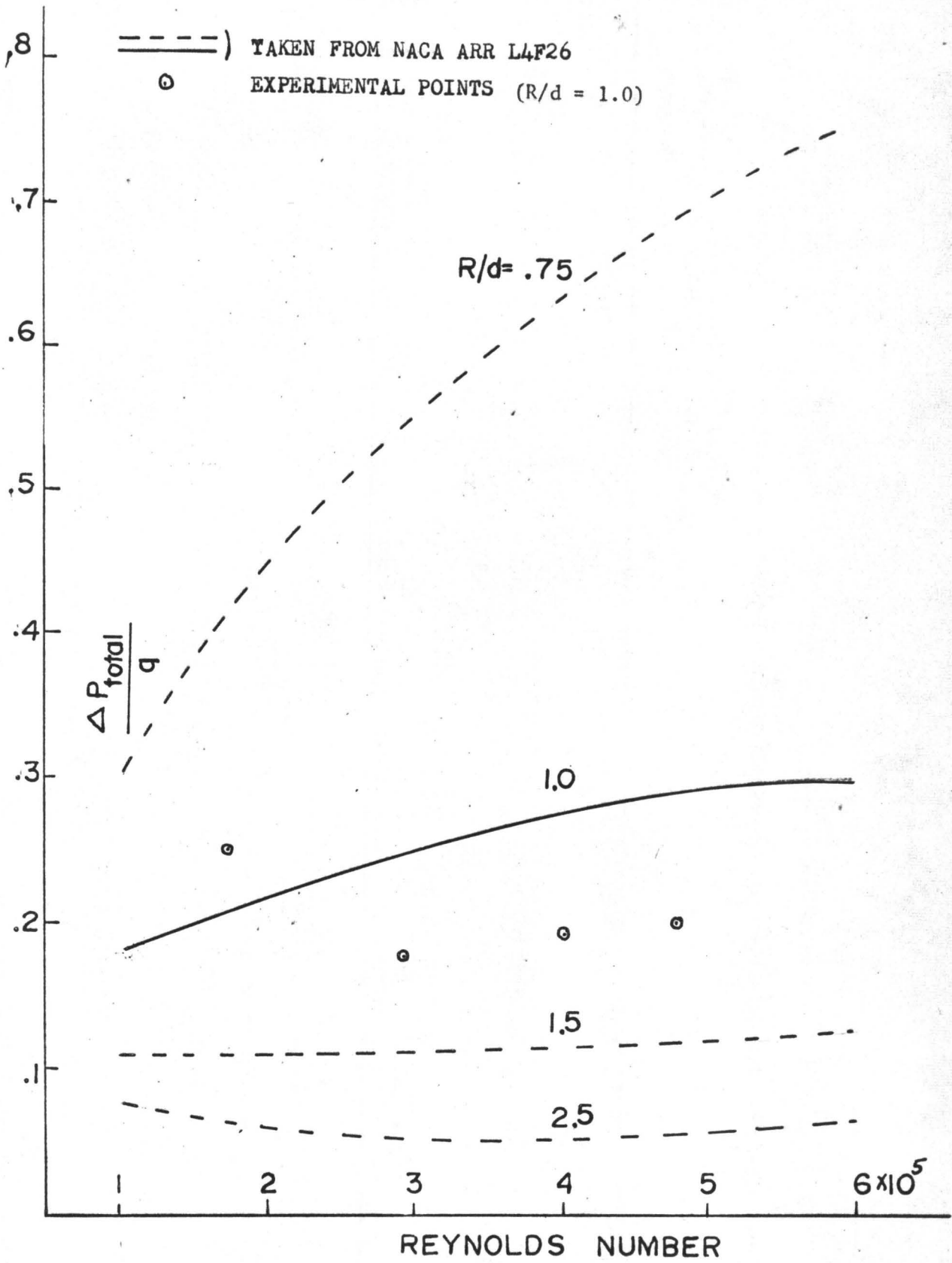TO PLENUM CHAMBER THROUGH 4D LONG DUCT FOR A=3

FIG.NO.28(c)

TOTAL PRESSURE LOSS ACROSS ELBOW WHEN IT IS DISCHARGING TO

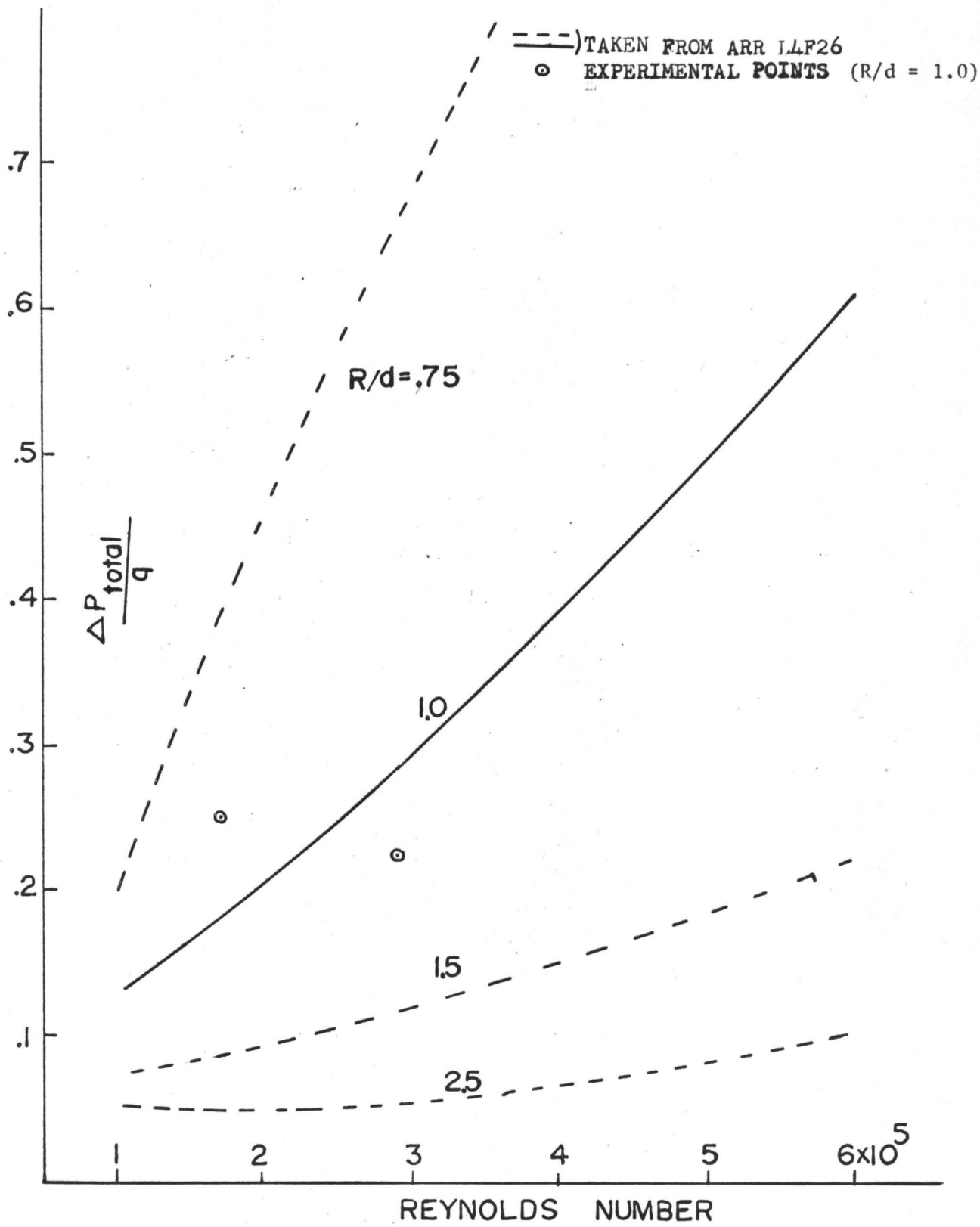PLENUM CHAMBER THROUGH 4 D LONG DUCT FOR A= 5

FIG.NO.28(d)

TOTAL PRESSURE LOSS ACROSS ELBOW WHEN IT IS DISCHARGING TO
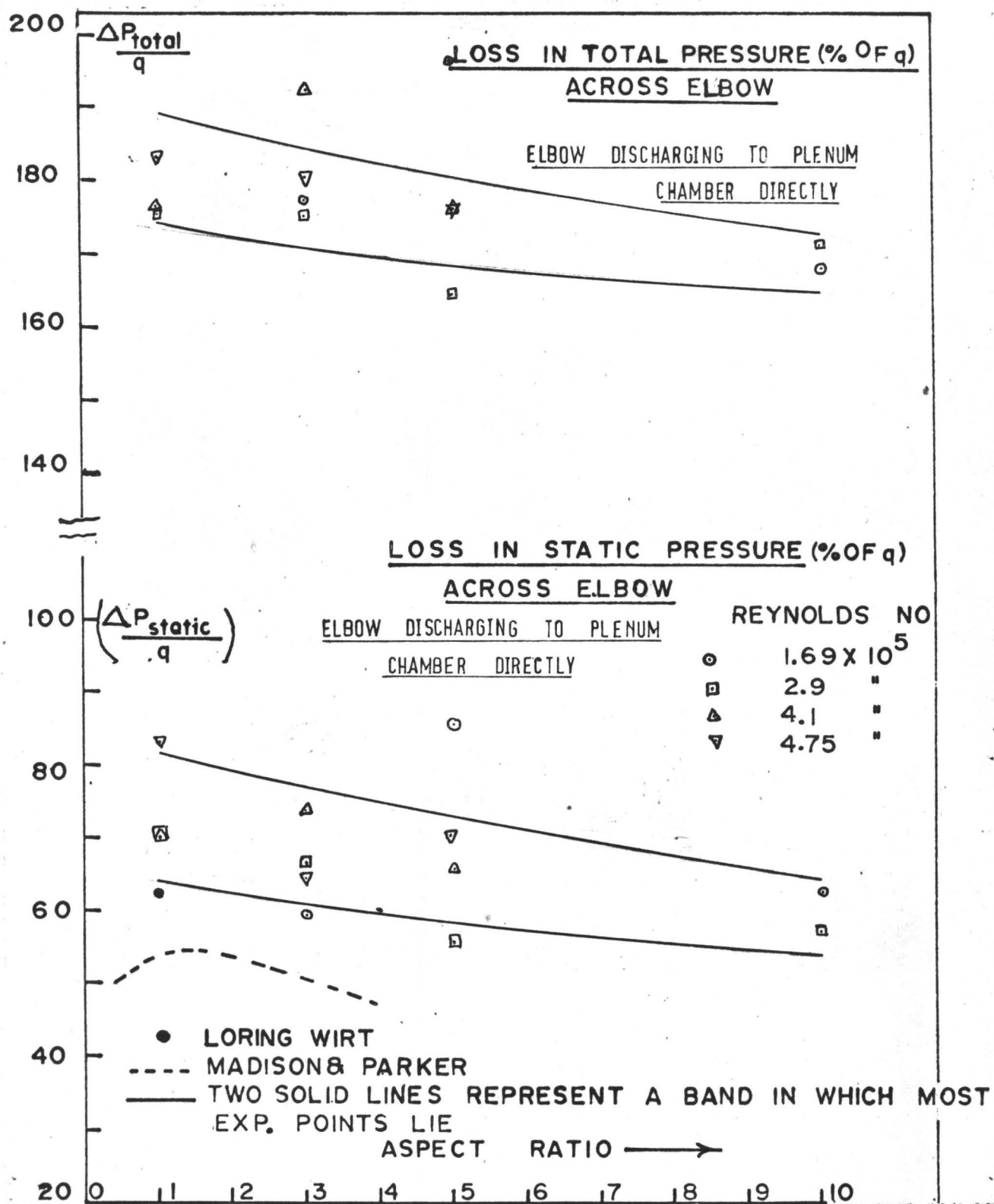PLENUM CHAMBER THROUGH 4 D LONG DUCT FOR A=10

FIG.NO.29

EXPERIMENTAL RESULTS OF THE LOSS IN TOTAL & STATIC PRESSURE

WHEN THE ELBOW IS DISCHARGING DIRECTLY TO PLENUM CHAMBER

APPENDIX NO. 1

Design of Contraction Cones

The contraction cones were designed on the basis of the wall profile given by Smith & Wang (23). They made use of exact analogy between the magnetic field that is created by two co-axial and parallel coils (Helmholtz) carrying electric current and the velocity field that is created by two ring vorticies. A family of these curves were developed and theoretical precision of uniformity of throat speed was also given. The design given was for three dimensional axi-symmetric nozzle. In the present work, four contraction cones were made corresponding to each set of experiments. Outlet section of these cones were (a) 24" x 24" (b) 24" x 8" (c) 24" x 4.8" (d) 24" x 2.4". Since the cross-section for the experiment at hand was rectangular, the profile of two sides of the cone (containing 24") were designed as given by Smith & Wang. Profile of other two sides were reduced as shown in following paragraph. Co-ordinates are also given. These contraction cones were made from 1/8 inch ply-wood sheet stiffened from outside to maintain the proper shape.
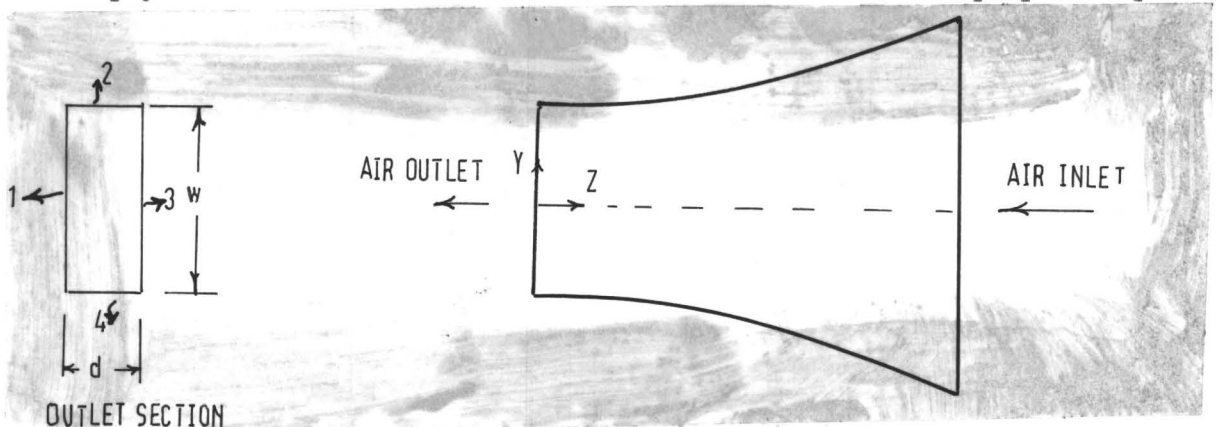
Aspect ratio A= w/d

d= w/A

w= 24" for all the four contraction cones

The design of contraction cone is divided into two parts. First the profile of the wall no. (1) & (3) will be given. Then the profile of walls (2) & (4) can be obtained from interpolation.

(a) Profile of faces (1) & (3): This is again divided into two parts. (a.1) For A= 3, 5, & 10: Curve J has been chosen from reference given previously. Uniformity of speed at outlet = 0.6%. Overall dimensions and coordinates are given below.

$$y_2 / y_1 = 71.48 / 24$$

$$= 2.97$$
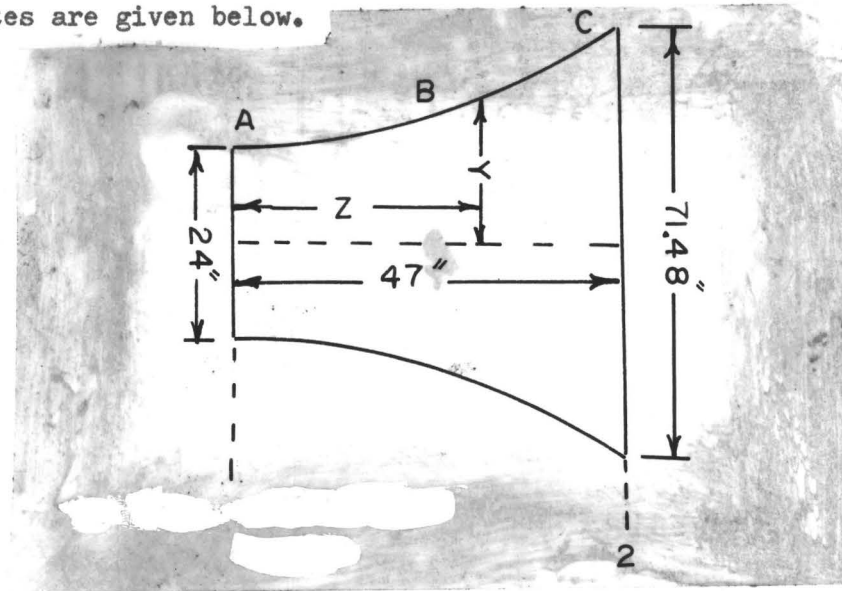
Z in Inches	Y in Inches
0	12.0
2.61	12.0
5.22	12.0
7.82	12.0
10.45	12.026
13.05	12.105
15.65	12.574
18.00	13.150
20.90	13.950

Z in Inches	Y in Inches
23.50	14.890
26.10	16.150
28.70	17.634
31.25	19.382
34.00	21.313
36.50	23,660
39.10	26.133
41.70	29.086
44.40	32.27
47.00	35.74

(a.2) For A=1: Curve l was chosen. Uniformity of speed=1%

$$y_2 = 45.0 \text{ in.}$$

$$y_1 = 24.0 \text{ in.}$$

$$z_2 - z_1 = 29.75 \text{ in.}$$

Coordinates are as follows:-

Z in Inches	2Y in Inches
0	24.000
2.4	24.000
4.8	24.000
7.2	24.000
9.6	24.288
12.0	25.056
14.4	26.256
16.8	27.888
19.2	30.048
21.6	32.688
24.0	36.00
26.4	39.84
28.8	43.256
29.7	45.000

Note: Profile given by l is slightly modified here.

(b) <u>Profile of Faces (2) & (4)</u>: This is again divided into two parts.

(b.1) For A= 3, 5 & 10
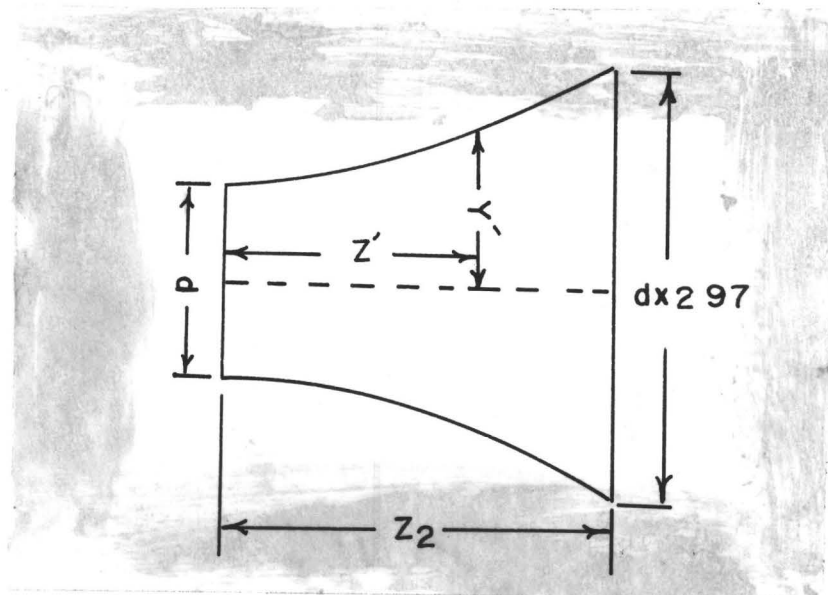
Z_2 = Curved length of profile for faces 1 & 3

  = Length ABC marked in part (a)

$Y' = Y/A$ ....   (Y is to be obtained from part (a))

(b.2) for A=1

  Profile given in part (a) is to be used because all the four faces are similar.

$$\underline{\frac{\text{INLET AREA}}{\text{OUTLET AREA}}} = 2.97 \times 2.97 \quad)$$
$$\qquad\qquad\qquad\qquad\quad) \quad \text{... For A= 3, 5, 10}$$
$$= 8.8 \qquad\qquad)$$

$$\underline{\frac{\text{INLET AREA}}{\text{OUTLET AREA}}} = 1.87 \times 1.87 \quad)$$
$$\qquad\qquad\qquad\qquad\quad) \quad \text{... For A= 1}$$
$$= 3.5 \qquad\qquad)$$

APPENDIX NO. 2

Turbulence Level

The level of turbulence is defined as $\dfrac{\sqrt{\overline{u'^2}}}{\bar{u}}$.

If $\sqrt{\overline{e'^2}}$ is rms voltage corresponding to $\sqrt{\overline{u'^2}}$ and $d\,E/d\,u$ is slope of d.c. voltage with respect to mean velocity $\bar{u}$ (calibration curve slope) then,

$$\% \text{ turbulence} = \frac{\sqrt{\overline{e'^2}} \text{ x } 100}{(d\,E/d\,u) \text{ x } \bar{u}} \quad \cdots\cdots\cdots (1)$$

King's Law states:

$$\frac{E^2}{R} = \alpha + \beta \sqrt{\bar{u}} \quad \cdots\cdots\cdots (2)$$

Where

$$E = \text{bridge voltage}$$

$$R = \text{probe operating resistance}$$

$$\bar{u} = \text{mean flow velocity}$$

α & β are two constants.

Equation no. (2) can be written as:

$$\frac{E^2}{R} = \frac{E_0^2}{R} + \beta \sqrt{\bar{u}} \quad \cdots\cdots\cdots (3)$$

Where E_o = bridge voltage at zero velocity.

From equation (2) taking the derivative one writes;-

$$\frac{2\,E}{R} \quad \frac{d\,E}{d\,u} = \beta \frac{1}{2\sqrt{\bar{u}}}$$

and $\therefore \bar{u} \quad \dfrac{d\,E}{d\,u} = \dfrac{\beta \quad R}{4\,E} \quad \sqrt{\bar{u}}$

But from equation (3)

$$\beta \sqrt{\bar{u}} \ R = E^2 - E_0^2$$

Thus,

$$\frac{d\,E}{d\,\bar{u}} \quad \bar{u} \quad = \quad \frac{E^2 - E_o^2}{4\,E} \quad \dots\dots\dots\dots (4)$$

Substituting equation (4) in equation (1) we get,

$$\% \text{ turbulence} \quad = \quad 100 \times \sqrt{\overline{e^2}} \quad \times \quad \frac{4\,E}{E^2 - E_o^2}$$

$$= \quad 100 \times E_{rms} \quad \times \quad \frac{4\,E}{E^2 - E_o^2}$$

APPENDIX NO. 3

Sample Calculations

The calculations for the loss in total and static pressures have been shown for the two cases.

Case 1: Elbow discharging to the plenum chamber through a straight duct of 4 hydraulic diameters.

Working fluid is air

Cross section of the duct	= 24" x 8"
Hydraulic diameter	= 1 ft.
Aspect ratio A	= 3
Radius ratio R/d	= 1
Speed of turbine	= 1550 rpm
Centre line velocity at Station 0	= 71.5 ft./sec.
At station 0 δ^* (outside wall)	= .09 in.
At station 0 δ^* (top wall)	= .07 in.

It is assumed that velocity profile is symmetrical and hence on other two wall displacement thickness is the same as given above.

Effective area = $(24 - 2 \times .07)(8 - 2 \times .09)$ in^2

= 23.858×7.82 in^2

= 1.29 sq. ft.

Geometric area = $(24 \times 8)/144$ sq. ft.

= 1.33 " "

$V_{av.}$ = $(1.29 \times 71.5)/1.33$ ft./sec.

= 69.65 ft./sec.

$$q \quad = \tfrac{1}{2} \, \rho \, V_{av.}^2 \qquad\qquad lbf/ft.^2$$

$$= \tfrac{1}{2}(.0735/32.2) \times (69.65)^2 \qquad "$$

$$= 5.536$$

$$= 1.058 \text{ in. of water}$$

Reynolds number $\quad = (\rho \, V_{av.} D)/\mu$

μ * at 80 degree F $\quad = .0185$ cp.

$$= 1.245 \times 10^{-5} \; lb_f/ft.sec.$$

$\rho/\mu \qquad\qquad = 5.91 \times 10^3 \; sec./ft^2$

Reynolds number $\quad = 4.1 \times 10^5$

From the measurements of the loss in total pressure between Station 1 & 13 (Horizontal and Vertical) mean effective loss is obtained by integration of graphs similar to Figure No. 27. This is given below:-

Horizontal mean effective loss in total pressure $\quad = .435$ in. H_2O

Vertical mean effective loss in total pressure $\quad = .33$ in. H_2O

Average loss in total pressure)
)
between Station 1 & 13 in inches) $\quad = \dfrac{.435 + .33}{2}$
)
of water)

$$= .382 \text{ in. of water}$$

From Appendix No. 4 loss in straight pipe of length 4 + 2½ diameter length at above Reynolds number is equal to .1015 inches of water.

Hence loss across elbow only $\quad = .382 - .101$ in. of water

$$= .281$$

Total pressure loss Coefficient K $\quad = .281/1.058$

$$= .265$$

---

*The physical properties of air were taken from "Handbook of Fluid Dynamics" by V. L. Streeter, McGraw Hill Book Company, Inc., 1961.

Case 2: Elbow discharging to the plenum chamber directly.

From measurements:

Average box static pressure   = 2.115 in. of water

Average static pressure at   = 1.325 in. of water
station 1

Average total pressure at   =   .086 in. of water
station 1

Hence, $\triangle P_{static} /q$ = (2.115 - 1.325)/1.058

                                      =   .746

                $\triangle P_{total} /q$ = (2.115 - .086)/1.058

                                      = 1.92

APPENDIX NO. 4

Friction Factor for the Duct

The friction factor has been determined across a straight duct of 8 feet in length. Table No. 1 gives the measured values of the loss in total pressure and calculated f for the duct cross section of 8" x 24" corresponding to aspect ratio of 3. With the values of f and Reynolds number from the Table 1, one can obtain values of the ratio ϵ/D using a Moody diagram. The values of ϵ/D was found to lie between .00005 to .0001. Hence ϵ lies between .00005 to .0001 feet. This value of ϵ corresponds to a duct which is very nearly smooth.

A further check was made for a duct of cross section 24" x 2.4" with aspect ratio of 10 and duct length of 8 feet. For this configuration the hydraulic diameter was .363 feet and the L/D equal to 22. Measured values of loss in total pressure and calculated f are given in Table No. 2.

If one assumes a value of ϵ as found from the measurements in Table 1 (for duct cross section 24" x 8") then the loss in total pressure for 24" x 2.4" duct can be calculated from a Moody diagram and these values can be compared with the experimental values given in Table No. 2. For example with an aspect ratio of 10 the limits of ϵ/D were found to be .000276 to .0001375.

Table No. 3 gives the value of f calculated from Moody diagram. The values of the friction factor in Table 3 agree with the values in Table No. 2 within 8%. This is the maximum possible error.

TABLE I

DUCT CROSS SECTION 8"×24"

HYDRAULIC DIAMETER I FT.

REYNOLDS NUMBER	ΔP_{total} BETWEEN STATION 0 & 1	$f = \dfrac{(\Delta P_t/q)}{(L/D)}$
1.75×10^5	.025 IN. OF WATER	.0161
2.80×10^5	.063 " "	.0161
4.10×10^5	.125 " "	.0148
4.75×10^5	.160 " "	.0142

TABLE 2

DUCT CROSS SECTION 2.4"×24"

HYDRAULIC DIAMETER .363 FT.

REYNOLDS NUMBER	ΔP_{total} BETWEEN STATION 0 & 1	$f = \dfrac{(\Delta P_t/q)}{(L/D)}$
1.69×10^5	0.52 IN. OF WATER	.0176
2.90×10^5	1.58 "	.0175

TABLE 3

REYNOLDS NUMBER	f CALCULATED FROM MOODY DIAGRAM	
	$\in/D = .000276$	$\in/D = .0001375$
1.69×10^5	.0180	.0170
2.9×10^5	.0172	.0160

APPENDIX 5

LOSS IN TOTAL PRESSURE ACROSS ELBOW

THE LOSS COEFFICIENT IS GIVEN BELOW WHEN ELBOW IS DISCHARGING TO THE BOX THROUGH 4 D LONG DUCT

A	REYNOLDS NUMBER	CENTERLINE VELOCITY AT STATION NO-O	q IN INCH OF WATER	ΔP_{total} IN. OF WATER	$K = \dfrac{\Delta P_{total}}{q}$
	1.69×10^5	14.75 FPS	.044	.0163	.37
1	2.9	25.0	.1318	.0482	.365
	4.1	35.5	.262	.076	.293
	4.75	42.4	.369	.096	.268
	1.76	30.5	.1948	.054	.273
3	2.82	48.5	.498	.152	.305
	4.1	71.5	1.058	.28	.265
	4.75	82.5	1.416	.40	.282
	1.69	42.5	.394	.10	.25
5	2.9	73.4	1.21	.21	.173
	4.1	103.6	2.35	.44	.19
	4.75	122.5	3.3	.66	.20
	1.69	77.8	1.34	.33	.25
10	2.9	134.5	4.05	.91	.224
		NO	DATA		

APPENDIX NO. 6

Solution of Laplacian Equation

If the flow in the bend is assumed to be incompressible, two dimensional and potential then, the Laplacian equation,

$$\frac{\partial^2 \psi}{\partial x^2} + \frac{\partial^2 \psi}{\partial y^2} = 0$$

is obeyed by the stream function. The above equation was solved by two methods - (a) Electric Analog Method and (b) Relaxation Method.

(a) Electric Analog Method

For a given configuration the electric potential can be regarded as the analog of stream function because it also obeys the same equation. In other words, constant voltage lines in an electric field correspond to constant stream lines in inviscid, incompressible and potential flow field provided that the boundary conditions are similar.

An analog field plotter was utilised to determine stream lines in the flow around the bend. The experimental arrangement is shown in the Figure 6.a (Appendix) with proper boundary conditions. As shown in the figure two inlet conditions were investigated. In the first case a uniform velocity was imposed at the inlet of the bend whereas in the second case a straight duct of length one equivalent diameter preceded and followed the bend with a uniform velocity simulated at the inlet and exit of these straight sections. With the help of a Wheatstone bridge employing a null indicator, constant potential lines were obtained which corresponded to the stream lines.

If 0 and 100% voltage is applied to the inner and outer walls
of the bend and no potential is applied across the inlet and outlet,
then the system will be analogous to the potential flow between con-
centric cylinders. The analytic solution for the stream function is
known for this case and it can be represented by ψ = constant $\ln r$.
Hence at the inlet and outlet ψ will not be linear and this of course
is a required boundary condition in our case. This simple example shows
the necessity of imposing a linear ψ at the inlet and outlet of the
bend to simulate uniform free stream velocity.

(b) <u>Relaxation Method</u>

Laplacian equation given in the previous section was solved
with proper boundary conditions on IBM 7040 computer.

For the first case when a uniform velocity was imposed at the
inlet and outlet of the bend, a rectangular grid of 29 x 29 was taken.
The position of the bend in this grid is shown in top of Figure 6.b
(Appendix). The intersection of the boundary with the grid is denoted
by EP & ET as shown in the figure. At each point in the grid, values
of EP & ET were supplied which defined the boundary lines. For all the
points which are inside the bend ET & EP = 1.0 and for the points lying
outside the bend EP & ET = 0. On the boundary of the bend values of
ET & EP lie between 0 and 1.0. Assumed values of ψ were supplied at
all interior points. This enabled one to reduce the computer time.
Relaxation in the area outside the bend and on the boundaries was
stopped by logic statements.

For the second case when a uniform velocity was imposed at the

inlet and outlet of the straight duct, a rectangular grid of 43 x 43 was employed. The position of the bend in the grid is shown in bottom of Figure 6.b (Appendix). The method of the solution was exactly the same as in the first case.

Accuracy of the solution can be increased by taking more points in the grid. But this required a compromise between the gain in accuracy and the computer time. Although no attempt was made to take a finer mesh and compare the two accuracies, it is felt that the present size of the grid gave good enough results from an engineering point of view.

Once the values of ψ were obtained at each point in the grid, the lines of constant ψ were drawn by linear interpolation. The next step was to obtain the pressure distribution from the stream lines.
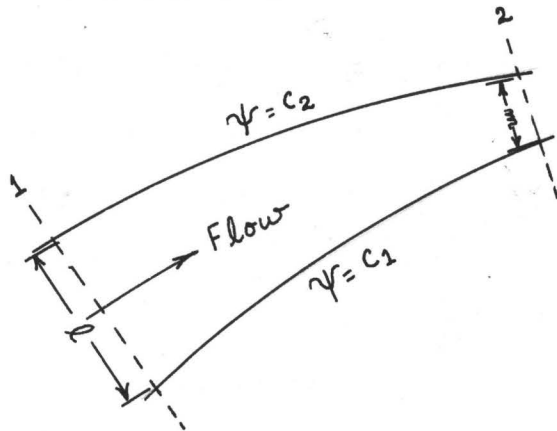
From the continuity equation,

$$V_1/V_2 = m/\ell = 1/n$$

Here it is assumed that the velocity does not vary across a section in the stream tube and the flow is incompressible.

From Bernoulli's equation

$$\tfrac{1}{2}\rho\,V_1{}^2 + p_1 = \tfrac{1}{2}\rho\,V_2^2 + p_2$$

$$p_1 - p_2 = \tfrac{1}{2}\rho\,V_2^2 - \tfrac{1}{2}\rho\,V_1^2$$

$$\frac{\triangle p}{\frac{1}{2} \rho V_1^{\,2}} = \left[\frac{V_2}{V_1}\right]^2 - 1$$

and therefore using the continuity equation

$$\frac{\triangle p}{q} = \left[n^2 - 1\right]$$

Pressure distribution along the walls of the bend was obtained by using the above equation.
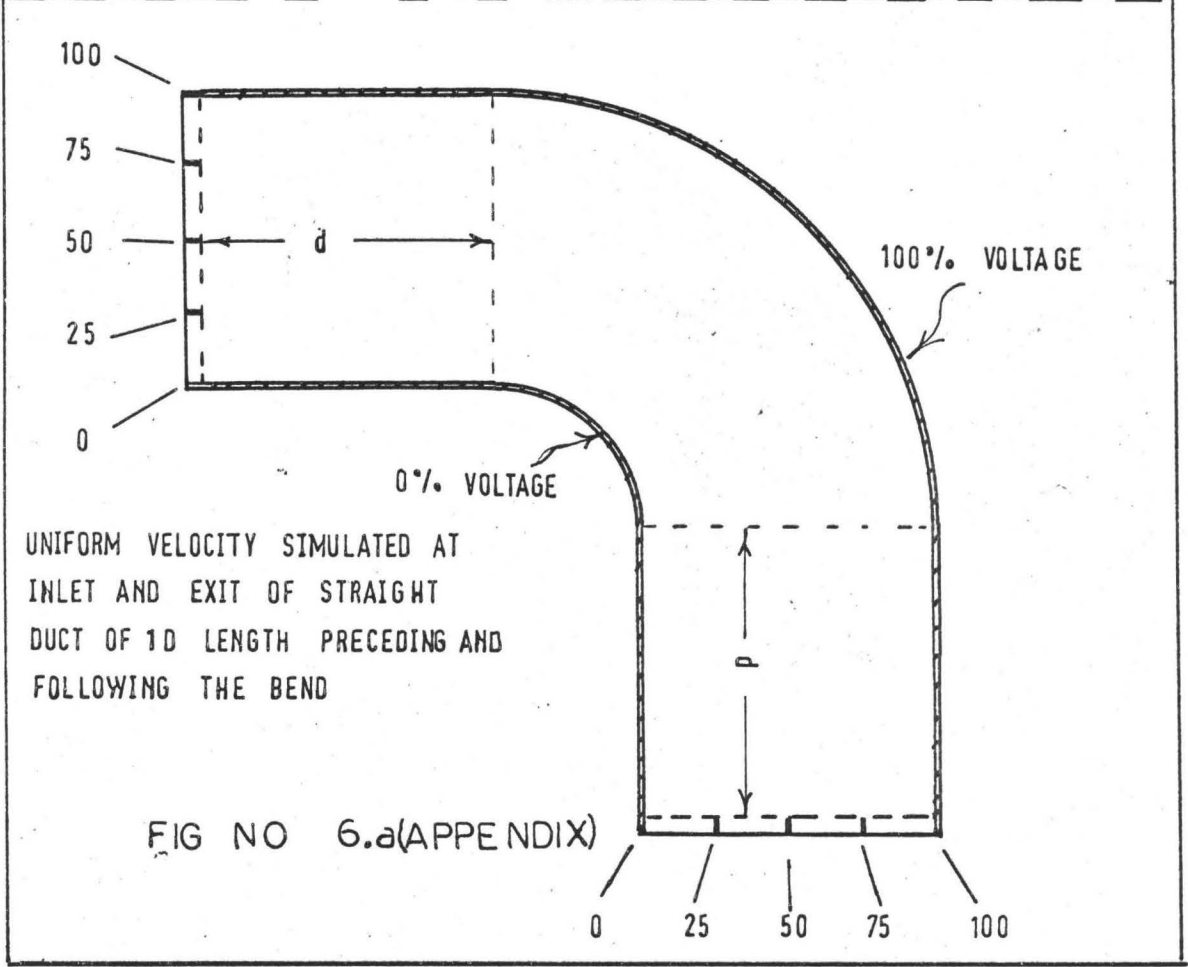
LINE VOLTAGE
SOURCE

R/d = 1

SILVER PAINT

UNIFORM VELOCITY SIMULATED
AT EXIT AND INLET OF BEND

NUMBER IN THIS FIG.
REPRESENTS VOLTAGE
IN %.

100% VOLTAGE

0% VOLTAGE

UNIFORM VELOCITY SIMULATED AT
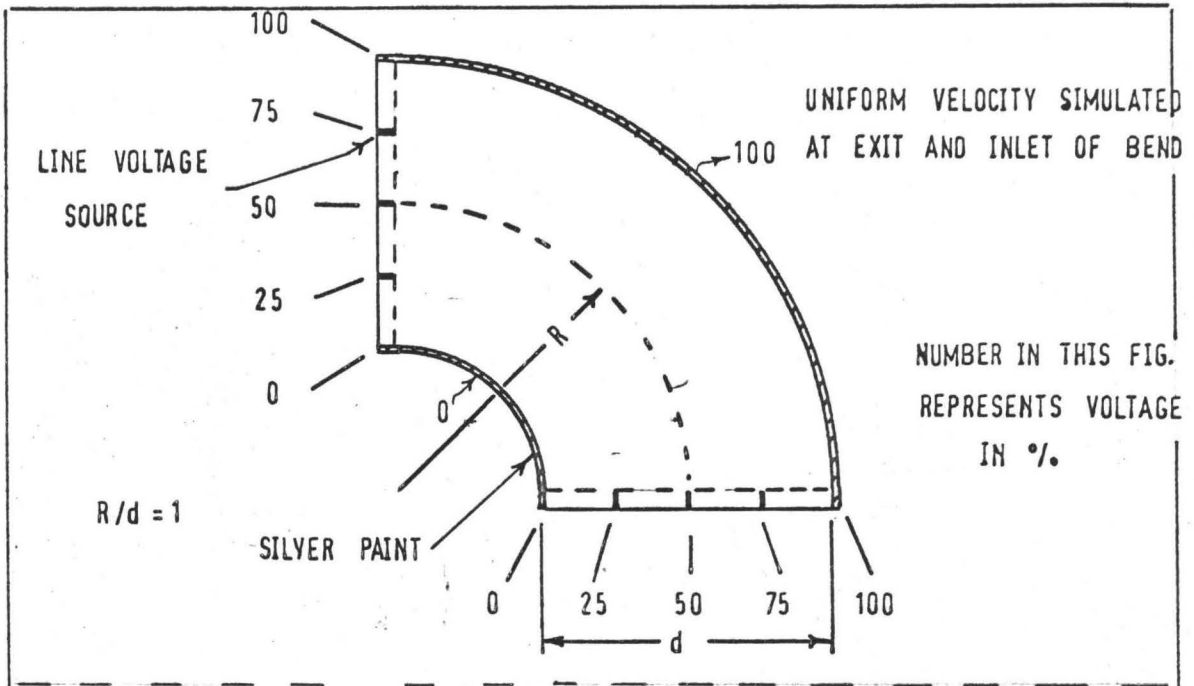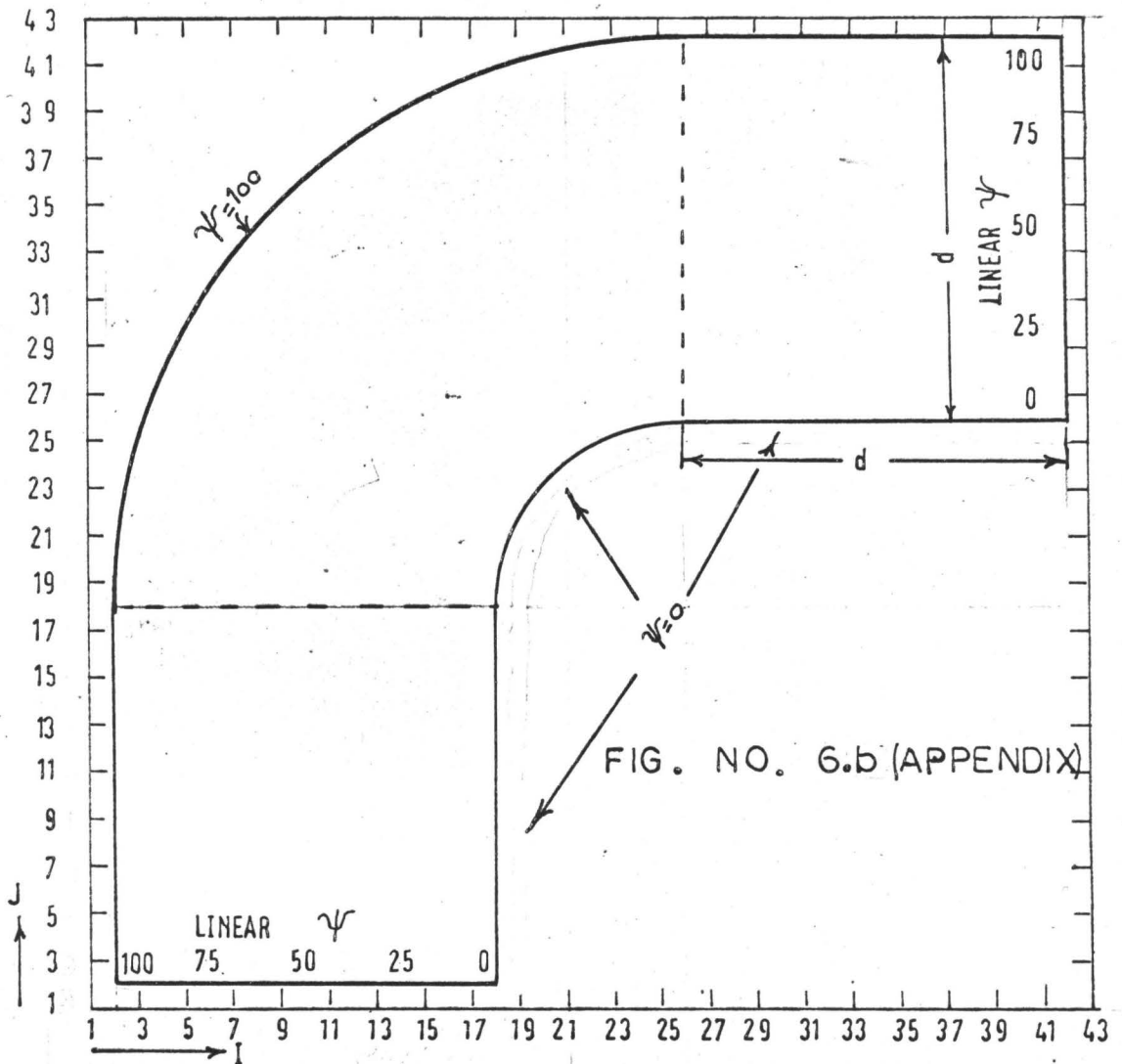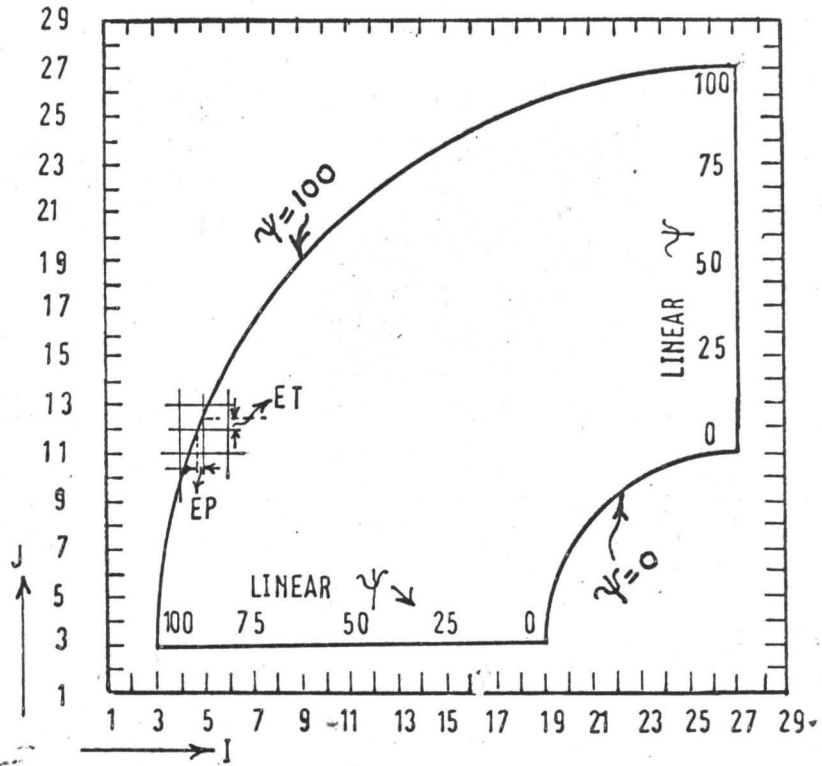INLET AND EXIT OF STRAIGHT
DUCT OF 1D LENGTH PRECEDING AND
FOLLOWING THE BEND

FIG NO 6.a(APPENDIX)

FIG. NO. 6.b (APPENDIX)